ADVANCED CERAMICS RESEARCH, INC.

Final Report

High Strength Carbide-Based Fibrous Monolith Materials for Solid Rocket Nozzles

Prepared for Missile Defense Agency under
Contract # HQ0006-05-C-7264

Submittal Date: February 19, 2008

Prepared by:

Jeanette M. Blaine, Mark Patterson
Advanced Ceramics Research, Inc.
3292 East Hemisphere Loop, Tucson, AZ 85706-5013

and

Xiaohong Zhang, Greg Hilmas, Bill Fehrenholtz
University of Missouri-Rolla, Department of Material Science and Engineering
223 McNutt Hall, Rolla, MO 65409-0340

REPORT DOCUMENTATION PAGE

Form Approved
OMB No. 0704-0188

PLEASE DO NOT RETURN YOUR FORM TO THE ABOVE ADDRESS.

1. REPORT DATE *(DD-MM-YYYY)*	2. REPORT TYPE	3. DATES COVERED *(From - To)*
19-02-2008	Final Report	30-09-2005 to 30-09-2007

4. TITLE AND SUBTITLE

High Strength Carbide-Based Fibrous Monolith Materials for Solid Rocket Nozzles

5a. CONTRACT NUMBER

HQ0006-05-C-7264

5b. GRANT NUMBER

5c. PROGRAM ELEMENT NUMBER

6. AUTHOR(S)

Jeanette M. Blaine, Mark Patterson, Xiaohong Zhang, Greg Hilmas, Bill Fehrenholtz

5d. PROJECT NUMBER

5e. TASK NUMBER

5f. WORK UNIT NUMBER

7. PERFORMING ORGANIZATION NAME(S) AND ADDRESS(ES)

Advanced Ceramics Research
3292 East Hemisphere Loop
Tucson, AZ 85706-5013

8. PERFORMING ORGANIZATION REPORT NUMBER

9. SPONSORING/MONITORING AGENCY NAME(S) AND ADDRESS(ES)

Naval Surface Warfare Center, Carderock Division Code 617
9500 MacArthur Boulevard
West Bethesda, MD 20817-5700

10. SPONSOR/MONITOR'S ACRONYM(S)

MDA/CTV

11. SPONSOR/MONITOR'S REPORT NUMBER(S)

12. DISTRIBUTION/AVAILABILITY STATEMENT

Distribution Statement A. Approved for public release; distribution is unlimited.

13. SUPPLEMENTARY NOTES

14. ABSTRACT

Two tertiary blends of tantalum carbide (TaC), hafnium carbide (HfC), and vanadium carbide (VC) have been developed for improved erosion and thermal shock resistance over current rocket nozzle materials for use with the "next generation" aluminized propellants. Advanced Ceramics Research's Fibrous Monolith (FM) technology has been used to produce structures with the developed high temperature carbide blend combined with a graphite intercellular layer. Monolith and FM materials have been evaluated at both room and elevated temperature. Both architectures show improved strength over TaC alone. High temperature evaluations performed at the Laser Hardened Materials Evaluation Laboratory (LHMEL) demonstrated significant improvements in thermal shock resistance with the FM material compared to monolithic structures.

15. SUBJECT TERMS

Tantalum carbide, Hafnium carbide, Fibrous Monolith, high strength, thermal shock resistance, solid rocket nozzle

16. SECURITY CLASSIFICATION OF:			17. LIMITATION OF ABSTRACT	18. NUMBER OF PAGES	19a. NAME OF RESPONSIBLE PERSON
a. REPORT	b. ABSTRACT	c. THIS PAGE			Jeanette M. Blaine
U	U	U	UU	66	19b. TELEPHONE NUMBER *(Include area code)* (520) 434-6363

Table of Contents

Background

"Next generation" aluminized propellants have become more energetic in order to impart a higher specific impulse to the system, resulting in higher temperatures and pressures that need to be contained. Nozzles are exposed to temperatures of up to 6100°F (3371°C) during aluminized propellant burn. Additionally, these propellants produce very hostile, abrasive environments; existing materials for boost throat applications have been shown to erode at unacceptable rates, leading to a loss in performance due to throat widening. Implementation of these propellants for boost and thrust applications requires the development of a new family of materials providing structural integrity, thermal protection, and low- or near-zero ablation rates above 3000°C. Erosion resistant nozzles which can maintain dimensional stability during firing are required.

Erosion in these systems can be attributed to the reactive environment, mechanical erosion, and spalling due to thermal shock. Appropriate material selection and architectural design can both be utilized to minimize erosion due to all three of these factors.

Ultra high temperature ceramics (UHTC) such as tantalum carbide (TaC) and hafnium carbide (HfC) are potential candidate materials for use in solid rocket nozzles. These materials have the highest melting points known, 3950°C and 3928°C, respectively. Compared to refractory metal candidates such as Rhenium (W) and Tungsten (W), these carbides offer significant weight savings. Densities for TaC and HfC are 12.2 g/cc and 14.3 g/cc, respectively, compared to 21.0 g/cc and 19.3 g/cc for Re and W. CVD coatings of these metals on bulk graphite nozzle mandrels, while providing significant cost and weight reduction, are susceptible to pinhole formation, delamination, and problematic CTE mismatches at elevated temperature.

Tantalum carbide (TaC) is stable to very high temperatures under non-oxidizing conditions found with aluminized propellants but is soft in its pure form and can erode appreciably. Improvements in strength and hardness can significantly decrease the susceptibility to mechanical erosion by molten alumina particles produced during the burn. Second phase additions of other refractory carbides have been shown in the Phase I program to significantly improve material hardness. Minimization and control of grain growth during manufacturing is another means of improving the strength of the material.

Monolithic UHTC components, although stable to high temperatures, are prone to catastrophic failure, particularly when subjected to impact or thermal shock. A fiber reinforced ceramic composite structure is expected to be more damage tolerant and resistant to thermal shock. However, these materials typically are not fully dense, making the part susceptible to accelerated erosion**.** The fibrous monolith (FM) architecture offers a significant mechanical improvement over a fiber reinforced ceramic material since the manufacturing process results in a fully dense material. The FM architecture consists of a major phase formed from a hard, strong ceramic material surrounded by a thin cell boundary of a weaker material. The structure provides internal

compliance and improved fracture toughness. Structural control can be used to manipulate the fracture behavior of UHTC materials without significantly altering the intrinsic properties or composition of the component.

In the Phase II program, both a materials development and architectural approach will be taken in order to optimize strength and erosion resistance of a TaC-based nozzle for boost applications.

Fibrous Monolith Processing

Fibrous Monolith (FM) processing (Figure 1) begins with the milling of commercially available powders or powder blends to produce mechanically activated and agglomerate-free powders. The individual powders are blended with thermoplastic melt-extrudable polymer binders and plasticizers, using a high shear mixer (Brabender Technologie Inc., Ontario, Canada) to form a smooth, uniformly suspended blend. The resulting mixture is pressed with heat into a feedrod core. A second material is blended separately and pressed into a thin shell designed to fit tightly around the core. Shells and core are combined to form a composite feedrod that is the basis for the FM process. This composite feedrod is extruded through a ram extruder to form a filament having the same volume ratios of the two constituents in the starting feedrod. These filaments can be chopped, bundled, combined with another shell, and extruded again to form a second pass extruded composite filament. The solids loading of the shell and core materials, volume ratios of the composite feedrod, and combinations of first and second pass co-extrusions can be varied systematically to change the properties of the composite. The flexible 'green' filament produced in the extrusion process can be woven, wound, braided, chopped (and pressed), or laid-up to produce a near net shape pre-form. Further consolidation is performed by a binder burnout process and final hot pressing. Additional machining may be required to achieve the desired tolerances of the final part.

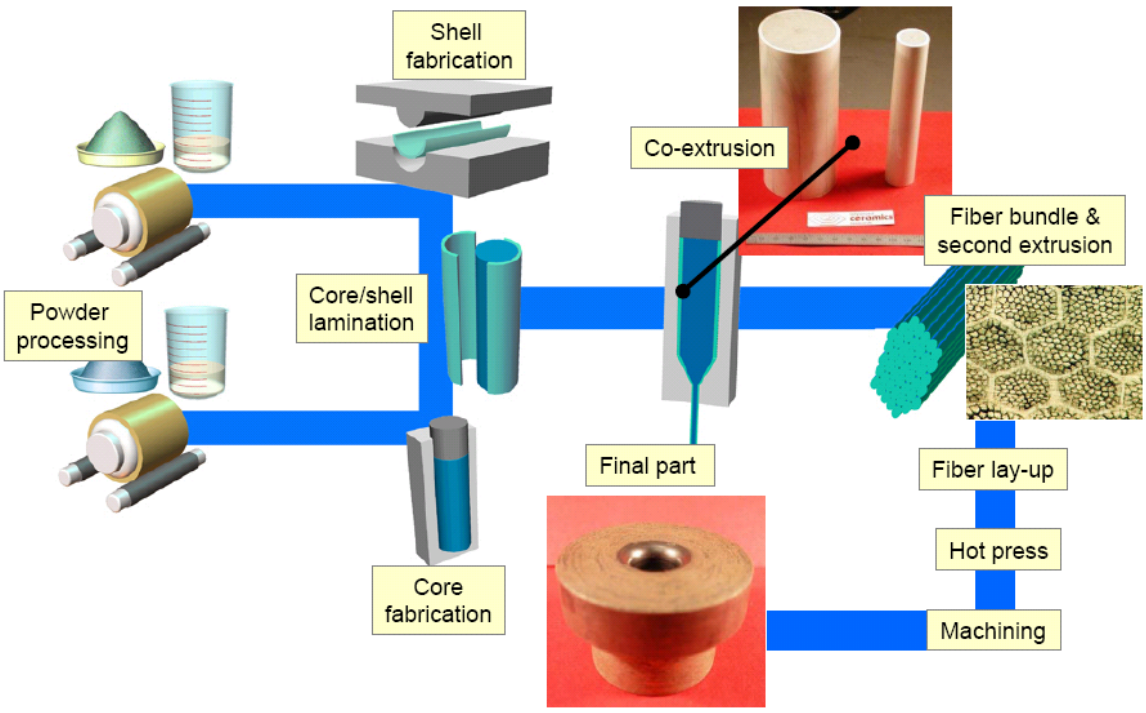

Figure 1. Fibrous monolith processing flow.

An advantage of the FM manufacturing process is the ability to easily form a variety of filament and final part architectures. Shell to core volume ratios, compositions, and dimensions can be adjusted easily in this process. Also, final parts with a variety of different architectures may be obtained. Filament may be wound around a mandrel as shown in Figure 2 to produce a nozzle with a concentric ring pattern. Billets of uniaxially aligned billets may also be cut into pie shaped pieces and arranged as depicted in Figure 3 to produce a radially aligned architecture with FM filaments arranged around the mandrel like the spokes of a wheel. Figure 4 shows two these different filament configurations used to produce solid rocket nozzles during this Phase II program.

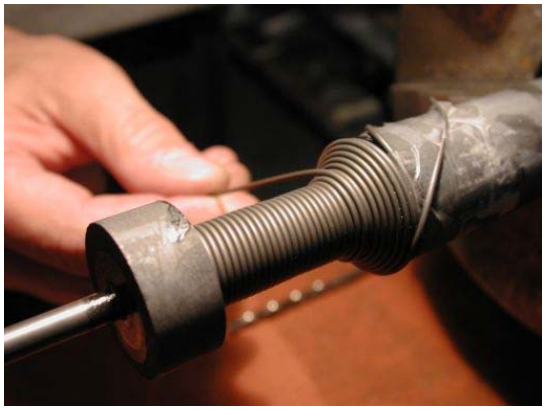

Figure 2. Fabrication of rocket nozzle by winding FM filaments around a steel mandrel.

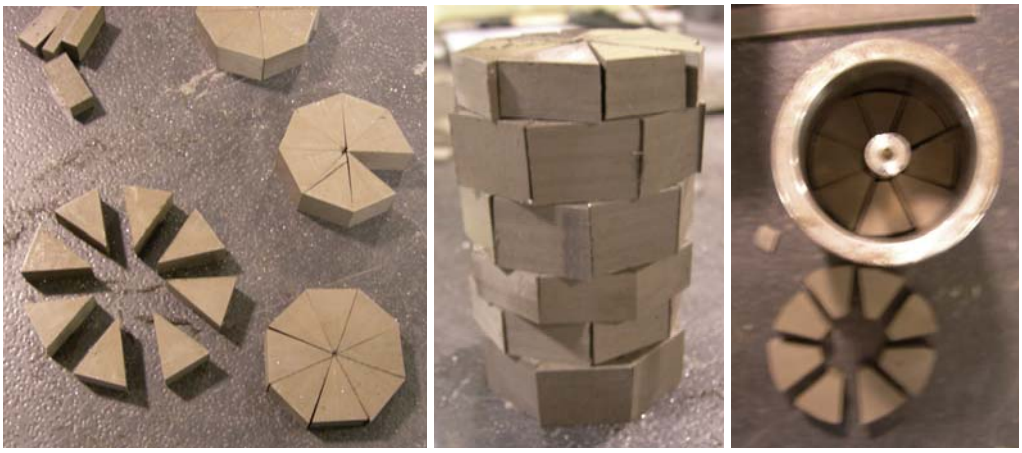

Figure 3. Fabrication of radially aligned, "pie" nozzle.

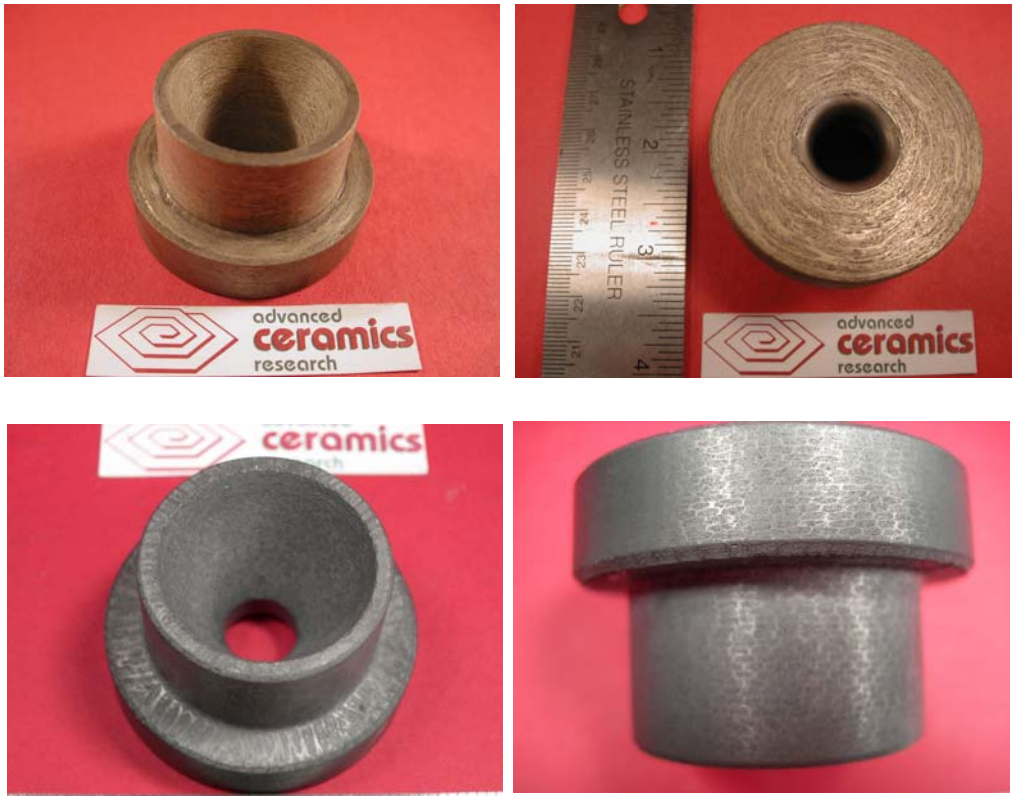

Figure 4. FM solid rocket nozzle architectures—wound filament (top) and radially arranged filament (bottom).

Phase II Technical Objectives

The objective of the MDA STTR topic (MDA04-T024) was to identify techniques to improve the strength of non- or low-erosion materials based on TaC or HfC. Significant strength improvements over the monolithic baseline are required for use in very high mass flux axial boost motor nozzles. These systems use aluminized propellants, producing a non-oxidizing environment. Boost Phase Intercept Missiles require

extremely high thrust axial motors in order to engage hostile targets in their boost phase. These motors operate at extremely high temperatures and pressures for short burn times (<10 seconds). To maximize the intercept missile performance, these materials must be thermal shock and erosion resistant in order to survive the high thermal stresses and minimize throat erosion which may lead to loss in performance.

In this Phase II program, the objective was to evaluate refractory carbide blends containing TaC and HfC in order to minimize erosion by increasing strength and hardness of the ceramic. The fibrous monolith architecture has been evaluated as a means of introducing some internal compliance into the structure, producing a part with improved thermal shock resistance capable of surviving the harsh aluminized propellant burn environment.

Experimental Procedure

Two different tertiary blends of TaC, HfC, and vanadium carbide (VC) were the focus of the Phase II effort. The first of these is a balanced composition of TaC and HfC with a low weight percentage of VC. The VC is believed to act as a liquid sintering aid, minimizing porosity for a given hot pressing temperature while keeping the hot pressing temperatures low. The second blend evaluated has a more TaC-rich composition, with lower HfC and VC weight percentages.

Compositions Evaluated:

"Balanced blend": 45 wt% TaC- 45% HfC- 10% VC

"**TaC-rich blend"**: 79 wt% TaC- 19% HfC- 2% VC = 75 vol% TaC- 20% HfC- 5% VC

Constituent carbide powders were combined and milled using a jar mill for 48 hours in isopropyl alcohol with zirconium oxide milling media. Materials were recovered by evaporating off the milling solvent, dried, and were either used to produce monolithic parts or were incorporated into fibrous monolith material.

Fibrous monolith material was produced using both tertiary carbide blends. A graphite shell was used to produce a weak, compliant interface. The binder burnout (BBO) profile used during the FM process is presented in Table 1. Table 2 describes the hot press (HP) profile used for final consolidation of the FM parts. For monolithic materials, this same hot press profile is used. However, a peak pressure of 6 ksi rather than 4 ksi was used for monolithic components. Due to limitations of the HP furnace, a lower pressure was used to consolidate these typically larger FM materials. For both processes, BBO and HP, a nitrogen atmosphere was used.

Table 1. Binder burnout profile used for fibrous monolith materials.

Ramp (°C/hr)	Temp Level (°C)	Soak Time (hrs)
10	170	8
6	270	6
6	300	6
4	350	4
6	425	4
10	600	2
-	25	-

Table 2. Hot press profile used for fibrous monolith materials.

Ramp (°C/min)	Temp Level (°C)	Soak Time (min)	Pressure (ksi)
10	1000	15	0.5
10	1400	15	1
10	2100	60	4
-	25	-	4

The microstructure and room temperature mechanical properties of these two blends have been evaluated at ACR and at the University of Missouri-Rolla (UMR) as described below. Also, reactive additions of carbon and boron carbide (B_4C) to control grain growth and improve the densification of TaC-based materials have been evaluated at UMR. Results of these studies are fully discussed Appendix B. Room and elevated temperature mechanical properties of fibrous monolith samples have been evaluated at Southern Research Institute (SoRI). High temperature survivability of monolithic and FM materials has been evaluated by the Laser Hardened Materials Evaluation Laboratory (LHMEL) at Wright-Patterson Air Force Base.

Results and Discussions

Evaluations of Monolithic Blends

Balanced Blend: 45 wt% TaC- 45% HfC- 10% VC

Powder blends of 45 wt% TaC- 45% HfC- 10% VC were milled, recovered, and hot pressed to 6 ksi at ACR using a resistance heated furnace to temperatures ranging from 2000-2200ºC. Flexural strength measurements, x-ray diffraction (XRD) analysis of ground specimens, and scanning electron microscopy (SEM) were performed on each sample. Vickers' hardness and fracture toughness measurements were also conducted on polished samples.

Flexural Strength Measurement

Samples were evaluated using the Instron tensile testing apparatus. Flexural strength was measured on B-type bars (3 mm x 4 mm x 25 mm) using four-point flexure methods according to ASTM C1161. Data (Table 3) show increasing strength with hot pressing temperature.

Table 3. Flexural strength data for 45% TaC- 45% HfC- 10% VC blend

Sample ID	Hot Press Temperature (°C)	Flexural Strength (MPa)	Number of Samples
HP-1400	2000	483 ± 149	9
HP-1402	2100	519 ± 196	14
HP-1403	2200	715 ± 169	8

Microstructural Analysis

The fractured surface of the samples was observed by SEM (Hitachi S-570). Images of the fracture surfaces of samples hot pressed at 2000, 2100, and 2200ºC shown in Figure 5 reveal that fracture is predominantly intergranular. These images, taken at nearly the same magnification, show that the grain size of the TaC-HfC-VC material increases with hot pressing temperature from 2000 to 2200°C.

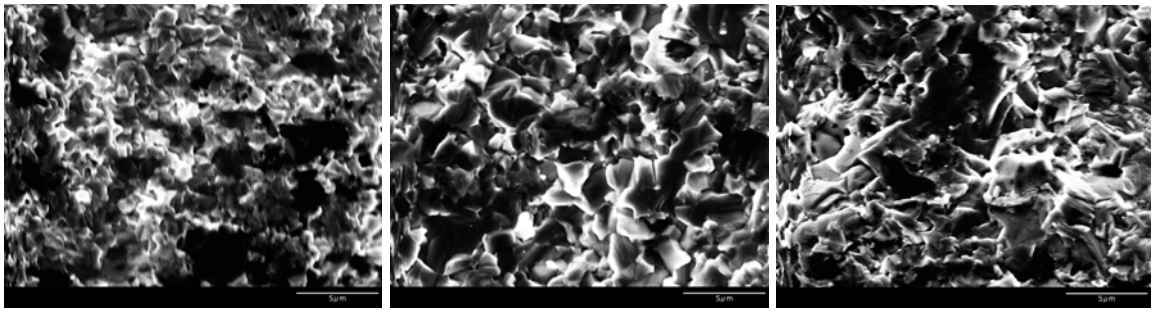

Figure 5. SEM micrographs of the fracture surfaces of samples monolithic 45 wt% TaC-45% HfC- 10% VC samples hot pressed at 2000°C (left), 2100°C (middle), and 2200°C (right).

In order to better reveal grain structure, samples were polished to a 1 μm finish using successively finer diamond abrasives then thermally etched at 1650ºC in argon for 1 hr. The microstructures of the etched surfaces (Figure 6) revealed the distribution of dark VC grains in the light grey TaC and HfC matrix. Vanadium, which has a much smaller atomic number than Ta and Hf, is easily distinguishable, producing a greater contrast in the SEM micrographs. Because of the similar atomic number of Ta and Hf, TaC and HfC grains would be difficult to distinguish from each other.

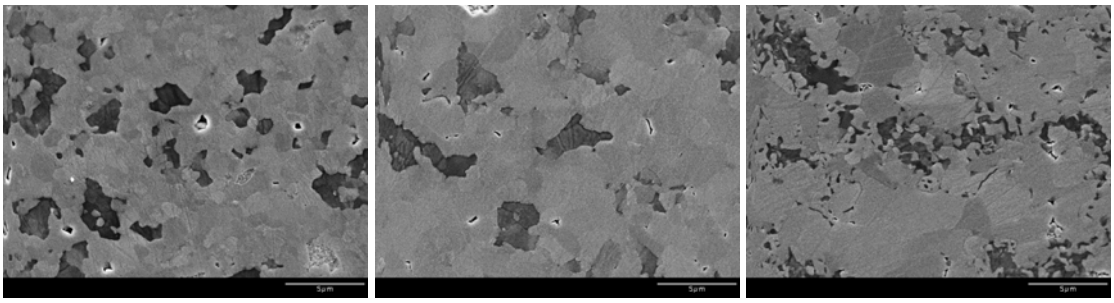

Figure 6. SEM micrographs of polished and etched surfaces of monolithic 45 wt% TaC- 45% HfC- 10% VC samples hot pressed at 2000°C (left), 2100°C (middle), and 2200°C (right).

The morphology of the structure suggests the formation of one or more solid solutions, which is not entirely unexpected for these materials. The three carbides are all cubic in structure. The lattice constant (Table 4) for HfC (4.644Å) is slightly larger (by ~4%) than that of TaC (4.4555 Å), which is again larger than that of VC (4.160Å) by about 7%. The covalent radius (Table 4) of Hf, Ta, and V decreases sequentially. Based on the similarity of the covalent radii and the lattice parameters, it appears that solid solutions should form readily among the three carbides.

Table 4. Lattice constants and covalent radii for constituents

Material	**HfC**	**TaC**	**VC**
Lattice constant (Å)	4.644	4.4555	4.160
Covalent radius of metal element (Å)	1.50	1.38	1.25

In general, the grain size of VC is larger than that of the TaC-HfC grains. Some level of porosity is observed in all of the samples. The samples hot pressed at 2000 and 2100ºC have a similar microstructure but overall larger grain size at 2100ºC (Figure 6). The sample hot pressed at 2200ºC (Figure 6) has a marked change in the resulting microstructure; the VC is no longer present as independent, equiaxed grains. It is apparent from the SEM analysis that there is an interaction between VC, TaC, and HfC materials.

XRD Analysis

Microstructural analysis revealed the possible formation of one or more solid solutions (ss) for the 45 wt% TaC- 45% HfC- 10% VC samples. A portion of each of the samples was crushed and passed through a 200 mesh sieve for powder XRD analysis (Scintag, XDS 2000, Cupertino, CA). The XRD patterns for samples HP-1400, 1402, and 1403 (Figure 7) indicate that the peaks are shifted from their original 2-theta positions when compared to the standard XRD patterns for pure TaC, HfC, and VC. This indicates the formation of one or more solid solutions.

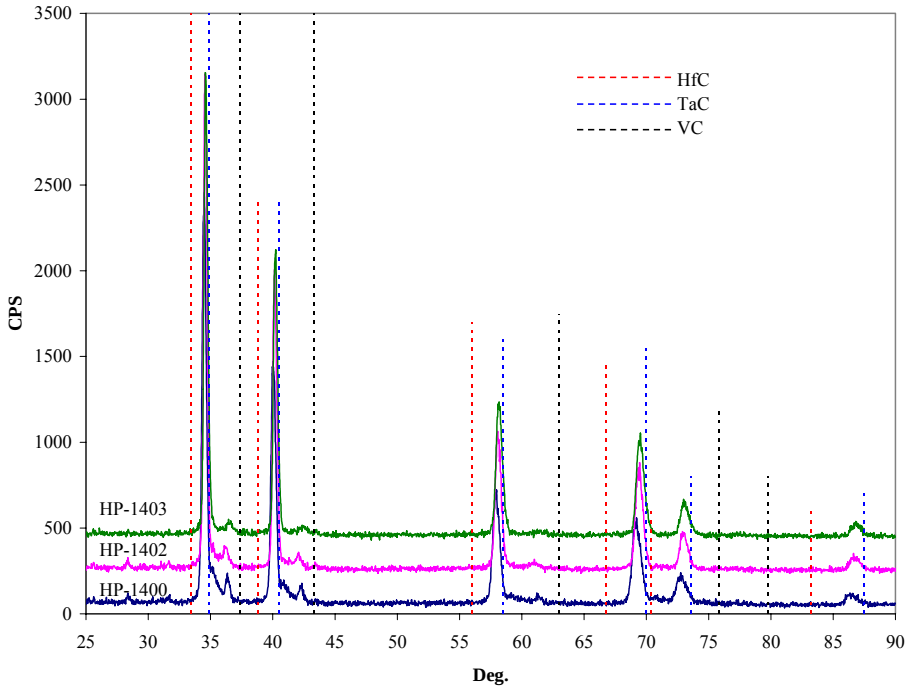

Figure 7. XRD patterns for 45 wt% TaC- 45% HfC- 10% VC materials pressed at 2000°C (HP-1400), 2100°C (HP-1402), and 2200°C (HP-1403).

The crystallographic plane d-spacings were calculated for these materials using Bragg's equation as follows.

$$\lambda = 2\ d \sin\theta$$

Where λ = 1.540562 Å, the wavelength of the incident x-ray radiation
d = d-spacing
θ = diffraction angle in degrees

Since all three constituents have cubic structures, the average lattice parameters for the hot pressed materials were calculated using the following equation.

$$\text{Lattice parameter, } a = d\sqrt{(h^2 + k^2 + l^2)}$$

Where d = d-spacing and h, k, l are Miller Indices for crystallographic planes.

Lattice parameters, shown in Table 5 decrease with increasing hot pressing temperature. This is consistent with infiltration of VC material into the matrix. This observation is supported by the reduced amount of "darker" phases present in the SEM micrographs shown in Figure 6.

Table 5. Lattice parameters for 45 wt% TaC- 45% HfC- 10% VC.

Sample	HP Temperature (°C)	Lattice Parameter (Å)
HP-1400	2000	4.4998
HP-1402	2100	4.4897
HP-1403	2200	4.4828

Hardness and Fracture Toughness Measurements

Hardness was measured using a 300 g load on a microhardness tester equipped with a Vickers' diamond indenter (Struers, Duramin-5, Ballerup, Denmark). The fracture toughness was measured using the direct crack measurement technique[1]. For fracture toughness measurement, polished samples were indented with a Vicker's diamond indenter under a 10 kg load (98 N) using the Leco hardness tester. The indents were then imaged using an optical microscope to assure that the load was sufficient to produce radial cracks extending from the indent corners with a total length (2c) that were a minimum of twice the length of the diagonal of the indents (2a). If adequate, crack length was measured. The fracture toughness was then calculated from the following equation.

$$K_{IC}=\zeta\left(\frac{E}{H}\right)^{1/2}\left(\frac{P}{c^{3/2}}\right) \qquad \text{[in MPa}\sqrt{\text{m}}\text{]}$$

where: E = the elastic modulus, GPa,
H = the hardness, GPa,
P = the applied force, kg
c = the length of the radial/median crack, μm
ζ = a dimensionless constant that has been determined from testing of many ceramics to be $\approx 0.016 \pm 0.004$.

The Young's modulus data used in the calculation were measured by ACR using the four-point bend test methodology. The elastic modulus, hardness, and the calculated fracture toughness values are contained in Table 6. The samples hot pressed at 2000 and 2100ºC had similar fracture toughness values of 2.4 to 2.5 MPa√m while the sample hot pressed at 2200ºC had slightly higher fracture toughness of 3.0 MPa√m.

Table 6. Fracture toughness measurements for 45 wt% TaC- 455 HfC- 10% VC material.

Sample	Hot Press Temp (°C)	E (GPa)	H (GPa)	K_{IC} (MPa√m)
HP-1400	2000	460	28.9	2.5
HP-1402	2100	476	30.3	2.4
HP-1403	2200	551	30.5	3

Additional SEM analysis was performed to observe the propagation of the radial cracks, produced during fracture toughness testing, through the microstructure. The images presented in Figure 8 shows the propagation of cracks indented using a 10 kg load. The cracks passed through some of the darker grains, thought to be vanadium-rich, but it is not clear if they passed through or around the lighter Ta-Hf-V-C (ss) material.

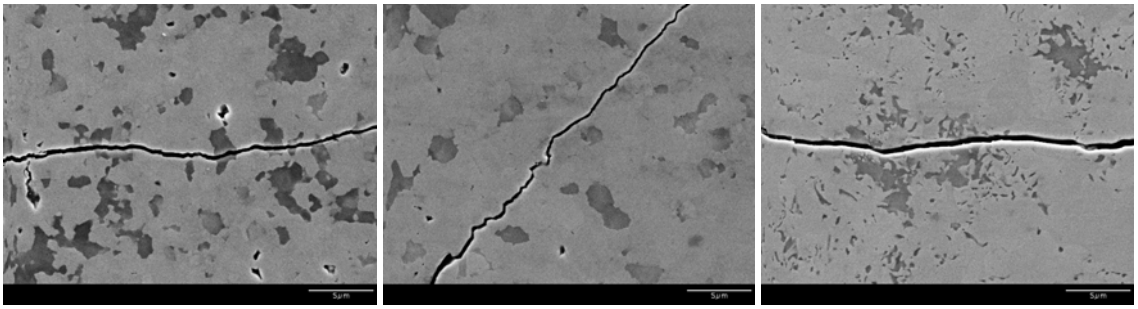

Figure 8. SEM micrographs showing the crack path from a radial crack produced by a Vickers' diamond indent at a 10 kg load in 45 wt% TaC- 45% HfC- 10% VC samples hot pressed at 2000°C (left), 2100°C (middle), and 2200°C (right).

TaC-Rich Blend: 75 vol% TaC- 20% HfC- 5% VC

Samples consisting of 75 vol% TaC-20% HfC- 5% VC, hot pressed at temperatures from 2000-2200ºC, were prepared by ACR as described above and tested by four-point flexure methods. Samples were sent to UMR for XRD, microhardness, and fracture toughness measurement. SEM microstructural analysis was performed on polished and samples that had undergone a thermal etch.

Flexural Strength Measurement

Flexural strength was measured using the Instron testing apparatus on B-type bars according to ASTM C1161. The data, shown in Table 7, show decreasing strength with hot pressing temperature.

Table 7. Flexural strength data for 75% TaC- 20% HfC- 5% VC blend

Sample ID	Hot Press Temperature (°C)	Flexural Strength (MPa)	Number of Samples
HP-1434	2000	741 ± 125	6
HP-1435	2100	545 ± 33	6
HP-1436	2200	487 ± 7	3

Microstructural Analysis

The samples were polished and then thermally etched at 1700°C in argon for 1 hour and examined by SEM. Micrographs of samples hot pressed at 2000, 2100, and 2200ºC shown in Figure 9 reveal the grain boundaries as well as some residual porosity. The sample hot pressed at 2200ºC contains more porosity than the other two samples, which is consistent with the trend in the flexural strength.

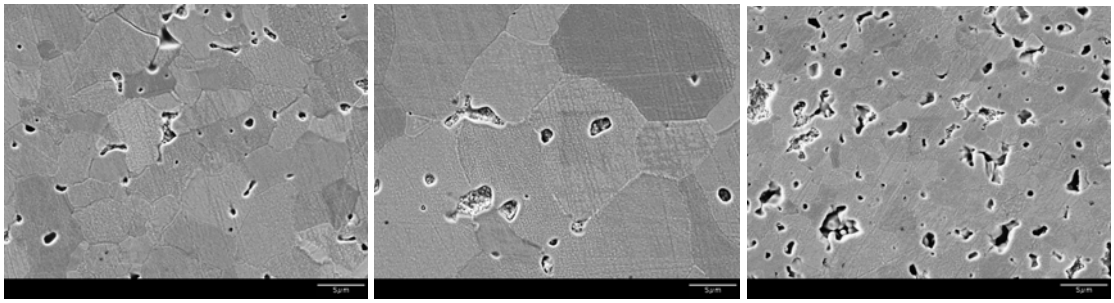

Figure 9. SEM micrographs of polished and thermally etched 75 vol% TaC- 20% HfC-5% VC material hot pressed at 2000°C (left), 2100°C (middle), and 2200°C (right).

There appears to be significantly more porosity in this high-TaC specimens compared to the more balanced blend discussed earlier. This may be attributable to the lower concentration (2 wt% compared to 10 wt%) of VC, thought to act as a liquid sintering aid, in these samples.

The presence of trapped porosity in all samples suggests that grain growth initiates at or even below 2000ºC and became rapid at 2100ºC with some of the pores becoming entrapped within the large TaC and HfC grains. The samples prepared at 2200ºC showed a very different microstructure from the other two samples. There seemed to be a lack of densification occurring at this temperature. There was no sign of grain growth and most of the porosity remained at the grain boundaries rather than entrapped within the grains. There is no clear explanation for this behavior at this time. Temperature and pressure logs for the hot press furnace indicate no anomalous conditions during the consolidation run.

XRD Analysis

XRD analysis was performed to determine the phases present in the samples. The XRD patterns (Figure 10) did not show a marked difference between the three hot pressing temperatures. The peaks were attributed to TaC with a slight shift of some peaks due to the formation of solid solutions. This tertiary composition is significantly more TaC-rich than the more balanced blend described earlier. Because of this, the shift observed in the diffraction patterns with this solid solution formation is markedly less dramatic.

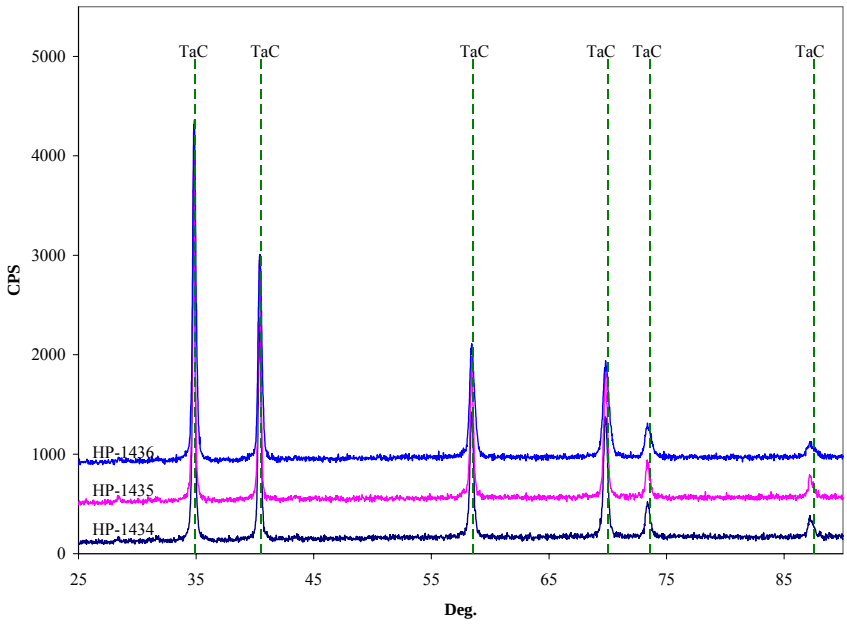

Figure 10. XRD patterns of 75 vol% TaC- 20% HfC- 5% VC samples hot pressed at 2000°C (HP-1434), 2100°C (HP-1435), and 2200°C (HP-1436).

The lattice parameters as a function of hot pressing temperature were calculated as described above and are shown in Table 8. These data further support the conclusion that a solid solution has formed. The lattice parameter calculated for all samples falls between that of pure TaC and HfC. The slight decrease in lattice parameter with hot press temperature is consistent with the incorporation of more of the V into the solid solution with hot press temperature.

Table 8. Lattice parameters of hot pressed 75 vol% TaC- 20% HfC- 5% VC samples.

Sample	HP Temperature (°C)	Lattice Parameter (Å)
HP-1434	2000	4.4680
HP-1435	2100	4.4676
HP-1436	2200	4.4650

Hardness and Fracture Toughness Measurements

Hardness and fracture toughness were measured as described above. Modulus values were obtained from four-point flexural strength tests conducted at ACR. The modulus, microhardness, indent load for toughness measurements, and the calculated fracture toughness values are contained in Table 9. The microhardness of samples prepared at 2000 and 2100ºC is approximately 22 GPa, higher than that of the sample prepared at 2200ºC which contained a higher fraction of porosity in the sample. The fracture toughness, approximately 4.4 MPa√m, was similar for all the three samples.

Table 9. Mechanical property data for 75 vol% TaC- 20% HfC- 5% VC material.

Sample	HP Temp (°C)	E (GPa)	H (GPa)	K_{IC} (MPa√m)
HP-1434	2000	471	22.7	4.5
HP-1435	2100	436	22.4	4.4
HP-1436	2200	411	19.4	4.3

Additional SEM analysis was performed to observe the propagation of the radial cracks, produced by a 10 kg load during fracture toughness testing, through the microstructure. The images in Figure 10 showed the propagation of cracks initiated by indentation with a 10 kg load. The micrographs show that the cracks tend to follow porosity in the indentation process.

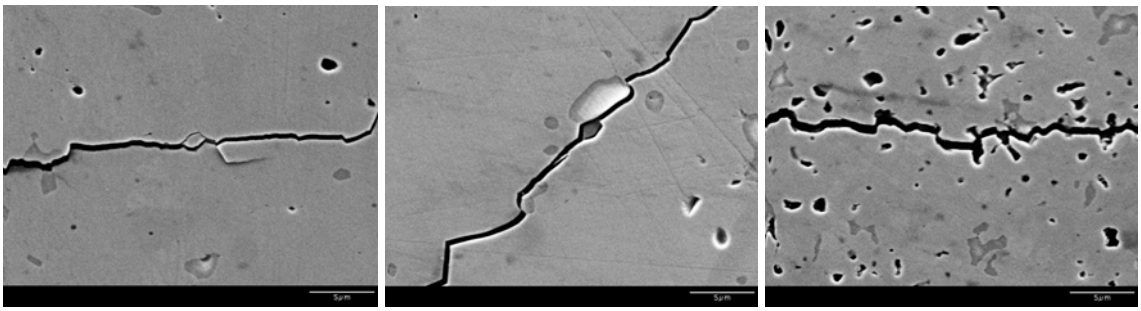

Figure 10. SEM micrograph showing the crack path from a radial crack produced by a Vickers' diamond indent at a 10 kg load in 75 vol% TaC- 20% HfC- 5% VC samples hot pressed at 2000°C (left), 2100°C (middle), and 2200°C (right).

Fibrous Monolith Evaluation at Room and Elevated Temperature

Fibrous monolith samples with TaC or TaC-HfC-VC phases and graphite interlayers were evaluated at SoRI. Initial samples evaluated were uniaxial structures with first pass extruded filaments as shown in Figure 11. Here, the core material is TaC and the shell material is graphite, providing a mechanism for internal compliance. The two tertiary blends developed during this program were evaluated using uniaxial lay-ups of second pass extruded filaments (Figure 11). Sample architecture is described in greater detail below.

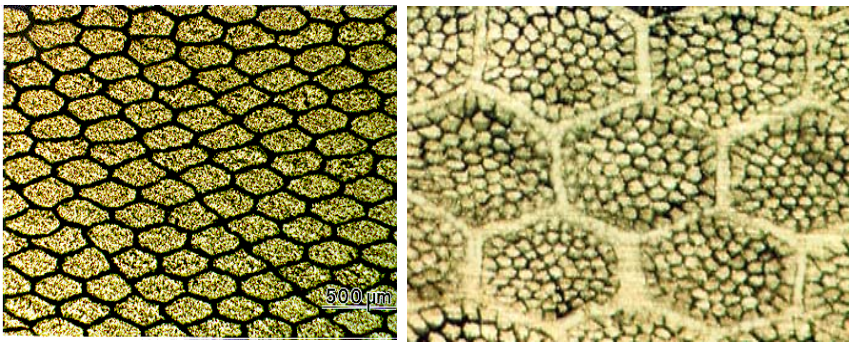

Figure 11. First pass (left) and second pass (right) FM architectures.

First and second pass composite green filaments were extruded to a 340 micron diameter and laid up in sheets to produce 8" x 2" x ¼" billets for testing. In the green filaments, a 17.5 vol% shell: 82.5 vol% core ratio was used. Sample details are specified in Table 10.

Table 10. FM sample configuration for tests performed at SoRI.

Sample ID	**HP #**	**Hot Press Temperature (°C)**
Gen 1: 1st pass TaC/graphite	1404, 1406	2200
Gen 2: 2nd pass TaC blend (45 wt% TaC- 45% HfC- 10% VC)/graphite/TaC blend	1430, 1431	2200
Gen 3: 2nd pass TaC blend (75 vol% TaC- 20% HfC- 5% VC) graphite/TaC blend	1440	2000
	1443	2100
	1445	2200

All samples were tested in tension and compression; longitudinal tensile strength, longitudinal Young's modulus, and transverse compressive strength were measured at room temperature (RT) and elevated temperature for all samples. High temperature testing was performed in a helium environment. Density and sonic velocity were measured for the Gen 3, TaC-rich material to determine the effect of hot pressing temperature on these physical properties. Data is summarized in Tables 11-13.

Table 11. Longitudinal tensile test data for FM samples.

Hot Press Temp (°C)	Test Temp (°F)	UTS (Ksi)	0.2% Yield Strength (Ksi)	Young's Modulus (Msi)	Strain-to-Failure (mils/inch)
Gen 1 : *1st pass TaC/ graphite*					
2200	RT	> 6.3*	-	-	-
		5.6	-	31.1	0.18
Gen 2 : *2nd pass 45 wt% TaC- 45% HfC- 10% VC / graphite*					
2200	RT	> 19.1*	-	46.2	> 0.41
		27.9	-	48.8	0.57
	3500	> 16.0*	14.9	9.2	> 5.7
		27.5	18.4	7.0	10.7
	4500	6.8	3.3	1.4	26.4
Gen 3 : *2nd pass 75 vol% TaC- 20% HfC- % VC / graphite*					
2000	RT	4.5	-	23.8	0.19
		4.5	-	26.7	0.16
	3000	-**	-	25.3	-
		7.6	-	16.5	0.46
		6.3	-	18.4	0.34
	3500	> 10.1**	-	14.7	-
2100	RT	7.5	-	27.4	0.27
		11.5	-	46.1	0.28
	3000	17.4	-	26.5	0.66
		15.2	-	28.7	0.64
2200	RT	> 14.9*	-	40.7	> 0.36
		22.9	-	57.8	0.42
		12.1	-	54.8	0.22
	3000	17.6***	-	37.4	0.47
	3500	> 9.4***	-	22.8	> 0.45

* Not ultimate strength or strain; specimen failed in loading pin holes or pullrod broke.
** Specimen loaded to 10.1 Ksi at 3500°F until loading pins broke. Sample retested at 3000°F using tungsten loading pens; specimen failed at 6.2 Ksi.
*** Specimen loaded to 9.42 Ksi at 3500°F until loading pins broke. Gauge width reduced and specimen tested to failure at 3000°F using tungsten loading pins.

The balanced blend Gen 2 material loses compressive strength when going from room temperature to 3500°F. This may be attributable to the higher concentration of V present in this material. The lower melting point of a VC phase may contribute to the weakening over this temperature increase. The strength of the TaC-rich Gen 3 materials is maintained over the temperature spread. Increased compliance of the material is observed with increasing temperature, however. All Gen 3 materials show significant decreases in modulus and strain-to-failure values at 3500°F.

The Gen 3 material has lower overall room temperature modulus values compared to the Gen 1 and Gen 2 materials. This may be attributed to poor consolidation of the Gen 3 material compared to the others. For the Gen 3 material, a notable increase in modulus is

observed with increasing hot pressing temperature. This trend is consistent with improved consolidation of the carbide/ graphite FM material.

Table 12. Transverse compressive test data for FM samples.

Hot Press Temp (°C)	Test Temp (°F)	Ultimate Compressive Strength (Ksi)	Young's Modulus (Msi)	Strain-to-Failure (mils/inch)
Gen 1 : *1st pass TaC/ graphite*				
2200	RT	21.8	32.2	0.78
		17.9	26.4	0.78
Gen 2 : *2nd pass 45 wt% TaC- 45% HfC- 10% VC / graphite*				
2200	RT	61.2	34.6	1.89
		61.9	32.1	2.06
	3500	25.1	10.9	25.9
Gen 3 : *2nd pass 75 vol% TaC- 20% HfC- 5% VC / graphite*				
2000	RT	13.6	10.6	1.40
		12.9	9.7	1.64
	3500	21.5	2.7	33.2
2100	RT	30.7	19.3	1.84
		30.1	15.8	2.10
	3500	28.3	7.7	14.6
		32.0	8.5	17.0
2200	RT	37.0	19.3	2.08
		51.8	29.9	1.84
	3500	33.4	9.4	18.1
		33.3	11.4	15.1

The effect of hot pressing temperature on the bulk density and sonic velocity of the Gen 3, TaC-rich FM material has been evaluated and is presented in Table 13. As the temperature used to consolidate the material increases, so does the density of the material. Sonic velocity, which has been measured along the length, width and thickness directions, increases as well with hot pressing temperature. This result is consistent with a decreasing level of porosity in the material.

Table 13. Bulk Density and Sonic Velocity of TaC-rich FM material as a function of hot press temperature (average of two data points per condition).

Hot Press Temp (°C)	Density (g/cc)	Sonic Velocity, Length (in/µsec)	Sonic Velocity, Width (in/µsec)	Sonic Velocity, Thickness (in/µsec)
2000	8.98	0.169	0.133	0.104
2100	9.90	0.198	0.160	0.119
2200	11.15	0.227	0.189	0.131

Summary of Test Results

Tensile testing was performed only in the direction of the filaments. The sample dimensions (2" wide, ½" thick) prevented tensile testing perpendicular to the filaments. Compression testing in the width direction was used to compare properties in the longitudinal and transverse directions. The FM material has proven inherently difficult to test in tension since the multilayered construction prevents use of round tensile specimens or flexure specimens and the brittleness makes it sensitive to corners and edges.

For the Gen 3 material, bulk density, sonic velocity, RT tensile strength, and RT Young's modulus increased with higher hot pressing temperature. This result may correlate with improved consolidation and decreased porosity with increasing HP temperature. The Gen 3 plate hot pressed at 2200°C had similar RT properties as the Gen 2 TaC. All Gen 3 materials had lower RT ultimate tensile and transverse compressive strengths than the Gen 2 TaC material hot pressed at 2200°C. At 3000°F, the Gen 3 plates hot pressed at 2100°C and 2200°C both had much better strengths and higher modulus values that the plate hot pressed at 2000°C. All Gen 3 material had lower strengths than the Gen 2 material at elevated temperatures as well.

The Gen 2 material was tested in tension at 3500°F but the others were tested in tension at 3000°F. Proper failure modes were not obtained at 3500°F for the other materials so direct comparison of the elevated temperature properties cannot be made. The Gen 2 material showed more strain capability at 3500°F than the other materials showed at 3000°F. Other bulk TaC materials have had a ductile to brittle transition temperature (DBTT) between 3000°F and 3500°F so a change in behavior of the Gen 3 material between these temperatures would be possible.

Microstructural Analysis of Tested FM Samples

The microstructure of select Gen 2 and Gen 3 samples, those with second pass FM architectures and one of the tertiary carbide blends investigated during the Phase II project, was investigated at the University of Missouri-Rolla (Table 14). Specimens were cut from the failed tensile bars and the fracture surface of each was examined using SEM. The microstructures of samples tested at room and elevated temperatures were compared.

Table 14. Tensile test samples evaluated using SEM.

Composition	**HP #**	**HP temp (°C)**	**Tensile test temp (°F)**
Gen 2: 45 wt% TaC- 45% HfC- 10% VC/ graphite FM	1431	2200	RT
	1431	2200	3500
Gen 3: 75 vol% TaC- 20% HfC- 5% VC/ graphite FM	1440	2000	RT
	1443	2100	RT
	1445	2200	RT
	1443	2100	3000

Balanced 45 wt% TaC- 45% HfC- 10% VC Blend/ Graphite FM Material

The architecture of the fibrous monolith filaments was still somewhat visible for sample 1431, hot pressed at 2200°C and tested at room temperature (Figure 12). The microstructure of the cells revealed extensive intragranular fracture. However, for the sample tested at 3500°F, a significant change was observed in the microstructure.

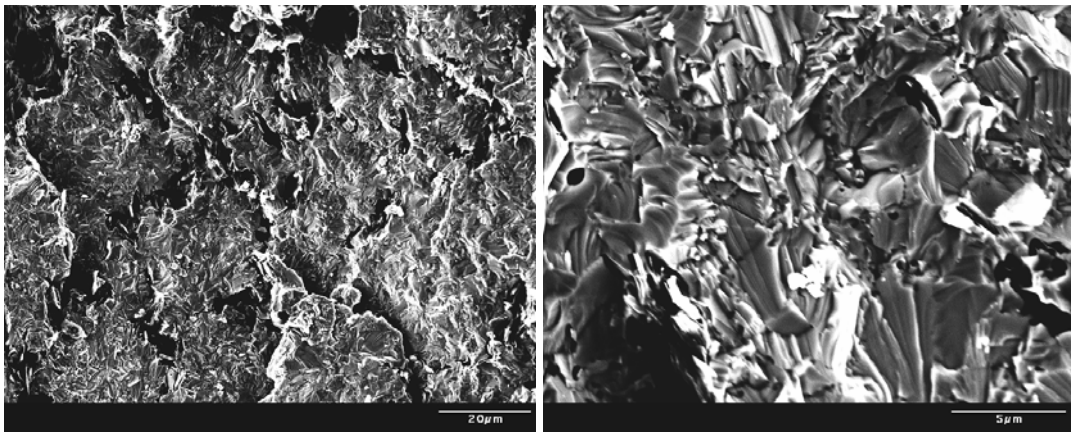

Figure 12. Fracture surface of 1431—45 wt% TaC- 45% HfC- 10% VC/graphite FM hot pressed at 2200°C— tested at room temperature

The architecture of the fibrous filaments was not discernable, possibly due to decomposition of the graphite at elevated temperatures (Figure 13). Higher magnification shows what appears to be severe microcracking within the grains. It is thought that an oxide layer has formed when the fracture surface was exposed at high temperature. The oxide layer subsequently cracked during cooling to room temperature, and due to the thermal expansion mismatch between the carbides and the oxide layer it has formed the unique microstructure on the fracture surface shown in Figure 13.

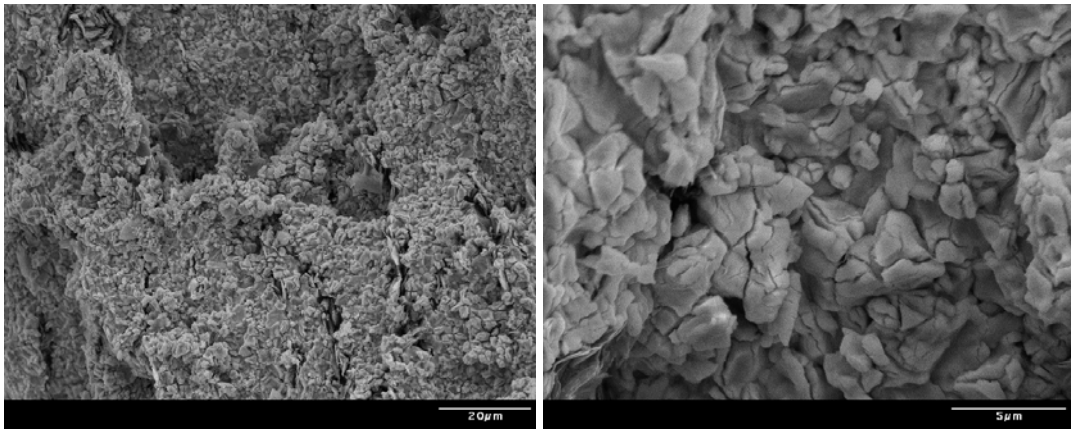

Figure 13. Fracture surface of 1431—45 wt% TaC- 45% HfC- 10% VC/graphite FM hot pressed at 2200°C — tested at 3500ºF

TaC-Rich 75 vol% TaC- 20% HfC- 5% VC Blend/ Graphite FM Material

The fracture surface of sample 1443, hot pressed at 2100°C, tested at room temperature shows that the architecture of the fibrous monolith filaments was retained (Figure 14). Higher magnification reveals the microstructure of the cells. The failure appears to be primarily intergranular. The grain size observed for this material is on the order of 1-2 microns.

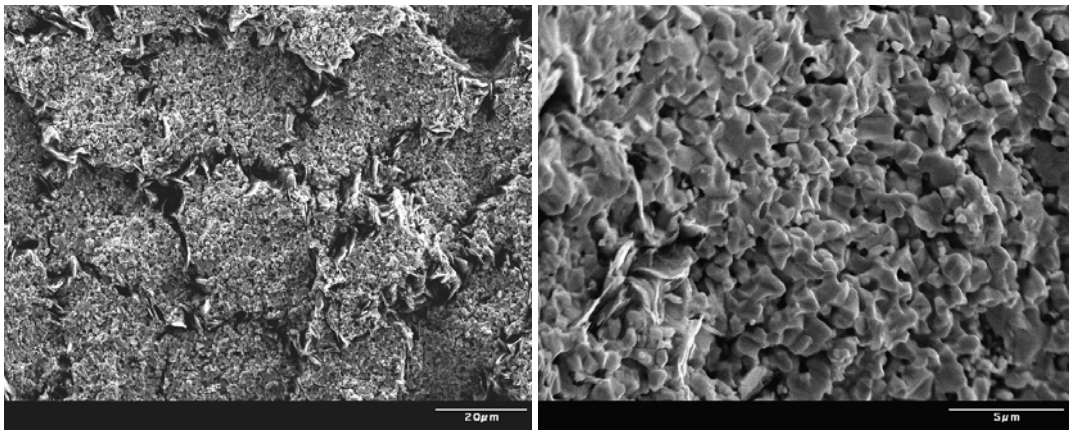

Figure 14. Fracture surface of sample 1443—75 vol% TaC- 20% HfC- 5% VC/graphite FM hot pressed at 2100°C— tested at room temperature

The FM architecture is not discernable in the sample tested at 3000ºF (Figure 15). Cell boundaries were not obvious as graphite may have decomposed at the test temperature. However, the microstructure of the cells did not change significantly. Intergranular failure dominates.

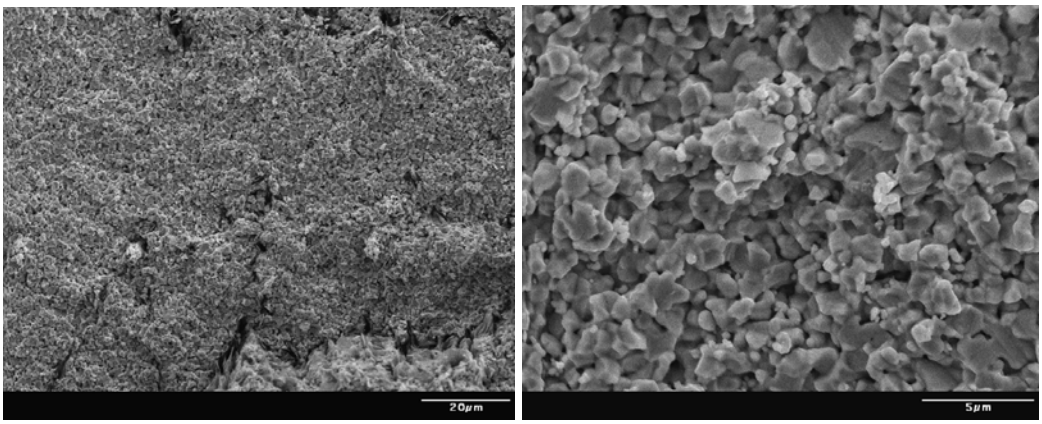

Figure 15. Fracture surface of sample 1443—75 vol% TaC- 20% HfC- 5% VC/graphite FM hot pressed at 2100°C —tested at 3000ºF

The fracture surface of sample 1445, hot pressed at 2200°C, tested at room temperature shows the retained FM architecture (Figure 16). Higher magnification reveals the microstructure of the cells, showing the presence of both intergranular and intragranular

fracture. The grain size (2-3 micron) observed for sample 1445 was slightly larger than that of sample 1443, hot pressed at 2100°C, tested at room temperature (1-2 microns). This result is probably due to the higher hot pressing temperature for sample 1445.

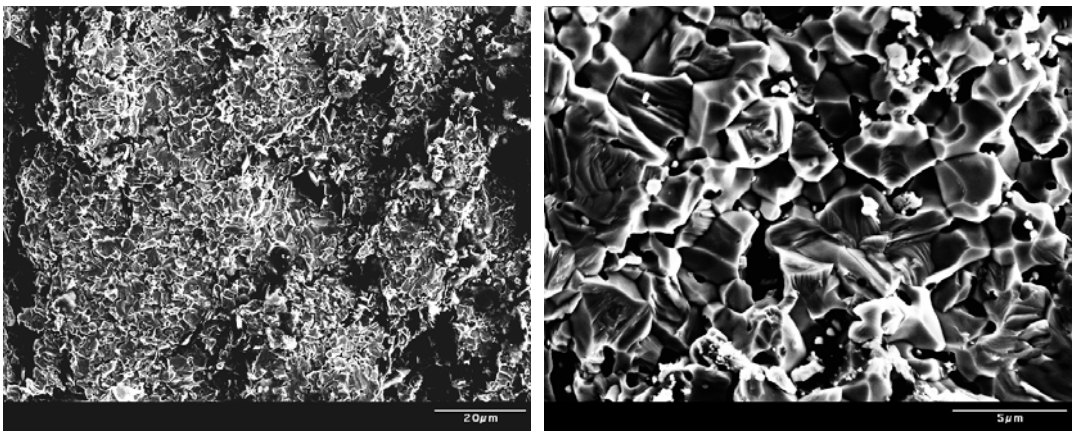

Figure 16. Fracture surface of sample 1445—75 vol% TaC- 20% HfC- 5% VC/graphite FM hot pressed at 2200°C—tested at room temperature

The fracture surface of sample 1440, hot pressed at the 2000°C and tested at room temperature, showed intact FM architecture in the sample tested at room temperature (Figure 17). Higher magnification, however, reveals poor consolidation at this hot pressing temperature; the microstructure of the cells is not fully dense. The grain size (1-2 micron) is similar to the material pressed at 2100°C. The sample failed in an intergranular manner.

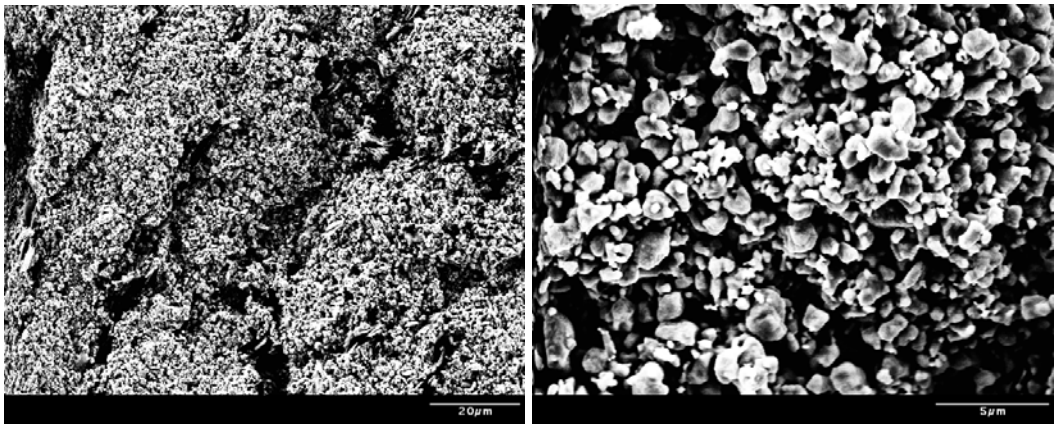

Figure 17. Fracture surface of sample 1440—75 vol% TaC- 20% HfC- 5% VC/graphite FM hot pressed at 2000°C—tested at room temperature

Flexure Strength of FM samples at Room Temperature

In addition, fibrous monolith samples of both tertiary carbide blend were machined into A-type bars (ASTM Standard C1161-02C; 1.5x 2x 25 mm bars) and sent to UMR for longitudinal flexure strength testing. The bars were polished to a 0.25 µm finish using

successively finer diamond abrasives. Flexure strength was measured in four-point bending in a mechanical load frame. A total of 6-9 bars of each composition were tested to obtain the average strength and a standard deviation.

The flexure strength data for the two compositions are shown in Table 15. Similar to what had been seen with the tensile and transverse compressive strength testing performed at SoRI, the strength of the more "balanced" composition (262 MPa) is higher than that of the "TaC-rich" composition (114 MPa). This may be attributable to the poor consolidation of the TaC-rich FM material. The fibrous monolith samples failed catastrophically in the flexural test; no graceful failure was observed although the samples were tested at a very slow crosshead speed (0.01 mm/min). Both samples are considerably less strong than their monolithic counterparts, a result that is expected when comparing the two different architectures.

Table 15. Flexure strength of fibrous monolith material hot pressed at 2100°C, 4ksi.

Composition	Flexure Strength (MPa)
45 wt% TaC- 45% HfC- 10% VC/ Graphite FM	262 ± 22
75 vol% TaC- 20% HfC- 5% VC/ Graphite FM	114 ± 31

High Temperature Evaluations at LHMEL

High temperature studies were also performed by the Laser Hardened Materials Evaluation Laboratory (LHMEL) at Wright-Patterson Air Force Base in Dayton, OH. The LHMEL I facility, with its 15kW continuous CO_2 laser, provides a relatively quick, inexpensive high temperature evaluation of the materials developed during this Phase II program. The objective of the experiment was to evaluate thermal shock resistance and survivability of ACR's materials in an oxygen deficient atmosphere, simulating conditions seen in systems using aluminized propellants.

Figure 18 shows the setup used during these evaluations. The 1.5" x 1.5" monolithic and fibrous monolithic specimens were mounted in a steel fixture, cushioned by graphite foam. The graphite foam was used to provide a less rigid support in case of thermal expansion as well as an oxygen gettering mechanism during the experiment. Front face temperatures were measured using a pyranometer during irradiation while backface temperatures were measured using a K-type thermocouple. Additional graphite foam was applied to the backside (not shown below) and a Mach 0.1 nitrogen flow was used to further reduce oxidation.

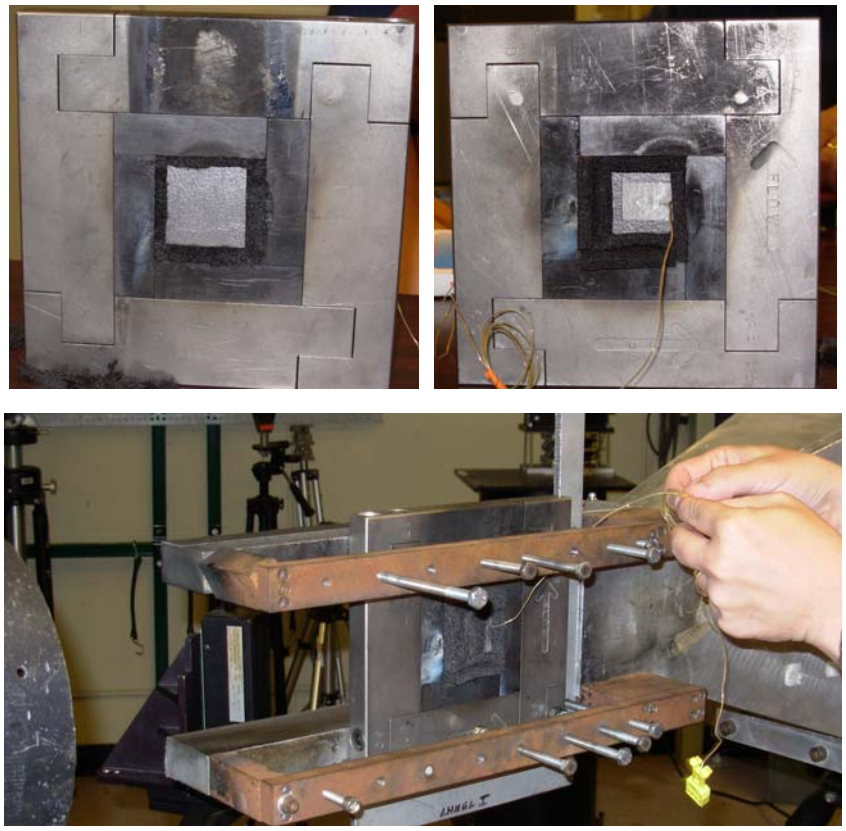

Figure 18. Experimental setup—front side (top left), backside (top right), and mounted in laser beam path with cross purge (bottom).

The conditions used to achieve temperatures in excess of 4000°F are described below. Samples were irradiated for 20 seconds. Front face and back face temperature data was collected during irradiation as well as during a 60 second cool down period. Except where noted, nitrogen flow was turned on during the entire 80 second period.

LHMEL I Experimental Specifications:
Flux: 1500 W/cm²
Spot size: 2.5 cm x 2.7 cm
Spot area: 5.3 cm²
Exposure time: 20s
Total Power: 8 kW
Purge: Nitrogen (99.99% pure), Mach 0.1

Both TaC-HfC-VC tertiary blends developed during the Phase II were evaluated. Monolithic and fibrous monolithic specimens were included; for the FM samples, both uniaxial and biaxial (0°/90°) samples were tested. The effect of sample thickness on high temperature survivability was also explored. Duplicates of each sample type, described below (Table 16), where performed where possible.

Table 16. Samples tested at LHMEL.

Carbide Blend	Architecture	Fiber Layup	Approx. Thickness
45 wt% TaC- 45% HfC- 10% VC	Monolithic	n/a	0.25”
	Fibrous Monolith	Uniaxial	0.1”
			0.25”
75 vol% TaC-20% HfC- 5% VC	Monolithic	n/a	0.25
	Fibrous Monolith	Uniaxial	0.1”
			0.25”
		Biaxial	0.1”
			0.25”

In general, the FM samples exhibited significant improvements in thermal shock resistance compared to their monolithic counterparts. For both blends, the monolithic samples cracked and failed catastrophically upon cooling and removal from the mount. The FM samples faired much better, with the TaC-rich samples performing much better than the balanced blend samples. For the TaC-rich FM samples, the thicker samples remained intact once removed from the mount and cooled, as did all of the thinner samples with the exception of one of the thinner uniaxial samples. All FM samples showed some cracking along the fibers. Ablation and cracking was observed for the balanced material. Thicker samples remained intact after cooling and removal from the mount. Thin samples, however, ablated so badly that the material had broken and blown out of the mount within the first 6 seconds of the test.

Temperature data and visual observations are detailed in Table 17 as follows. Complete front face and back face temperature profiles, pictures of the samples post-test, and microstructural analysis of several exposed samples can be found in Appendix A.

Table 17. Summary of LHMEL data.

Billet Type	Run #	Thx (in.)	Power (W/cm²)	Surface Peak Temp (°F)	Backface Peak Temp (°F) (1)	Comments
45 wt% TaC: 45 wt% HfC: 10 wt% VC						
Monolith	7061108	0.26	1479	5205	2570	catastrophic failure upon cooling/removal from mount, glassy appearance
	7061109	0.26	1486	5189	2546	catastrophic failure when removed from mount, glassy appearance
Uniaxial, thin	7061101	~0.13	1538	5259	2825	sample gone w/in 3s, ablated and blew away, none recovered
	7061115	~0.13	1529	4960	2439	sample gone w/in 6s, ablated and blew away
Uniaxial, thick	7061110	0.24	1475	4123	2278	backside delamination during heating, bulk stayed intact
	7061111	0.23	1503	5084	2277	delamination during heating, cracking during cooling
75 vol% TaC: 20 vol% HfC: 5 vol% VC						
Monolith	7061102	0.28	1493	4332	2563	catastrophic failure upon removal from mount, yellowing of surface (2)
	na	0.27	na	na	na	M.5 N_2 purge caused sample to fall to floor and break
Uniaxial, thin	7061113	0.12	1653	5016	2445	some cracking along fibers, sample stays intact
	7061114	0.12	1529	4818	2713	clean crack down middle of sample, along fiber
Uniaxial, thick	7061103	0.29	1507	4397	2390	surface yellow, no cracking observed, sample remains intact (3)
	7061105	0.30	1501	4551	2536	some cracking along fibers, through thickness, not catastrophic
Biaxial, thin	7061104	0.13	1514	5031	2559	some cracking along fibers, not catastrophic
	7061112	0.13	1503	4975	2453	some cracking along fibers, sample stays intact
Biaxial, thick	7061106	0.30	1506	4562	2412	some cracking along fiber on face side, stays intact
	7061107	0.31	1483	4966	2195	cracking along fibers, stayed intact until tugged apart for photos

(1) K-type thermocouple used melts at 2500°F
(2) Nitrogen purge turned off with laser, oxygen exposure during cool down caused surface reaction to occur.
(3) Nitrogen purge turned off with laser, restarted after approx. 15 seconds.

Conclusions

Two tertiary blends containing TaC, HfC, and VC have been evaluated. A TaC-rich blend, appropriate for an aluminized propellant application, and a more balanced blend, appropriate for a slightly more oxidizing reaction chemistry, have been evaluated. Mechanical strength and hardness of the monolithic materials, over TaC alone, have been achieved. This has been achieved by the introduction of HfC, a harder carbide, to the TaC system as well as the use of VC as a liquid sintering aid to help reduce the required consolidation temperature and minimize grain growth.

Fibrous monolith specimens have been evaluated at both room and elevated temperatures. Testing performed at the LHMEL facility showed that a significant improvement in thermal shock resistance has been obtained for the fibrous monolith samples over the monolithic ceramic parts. In an oxygen poor environment and at the temperatures achieved during the test, >4000°F, the TaC-rich tertiary blend showed better survivability over the more balanced blend.

A static firing test with an aluminized propellant would be an ideal test for the fibrous monolith materials developed during the Phase II. It is anticipated that the TaC-rich tertiary blend fibrous monolith material would show improved erosion and thermal shock resistance over the current baseline material.

Appendix A: High Temperature Evaluation at LHMEL

Below are surface and back face temperature profiles for samples tested at the LHMEL facility at Wright-Patterson AFB in Dayton, OH. Images of tested specimens after removal from the sample holder are also included. Microstructural analysis of selected samples is discussed throughout the text.

Monolithic and Fibrous Monolithic 45 wt% TaC- 45% HfC- 10% VC Material Evaluation

Figures A.1 through A.18 pertain to monolithic and fibrous monolithic specimens constructed using the 45 wt% TaC- 45% HfC- 10% VC blend developed during the Phase II program.

Figure A.1. Sample 07061108—Monolithic 45 wt% TaC- 45% HfC-10% VC sample.

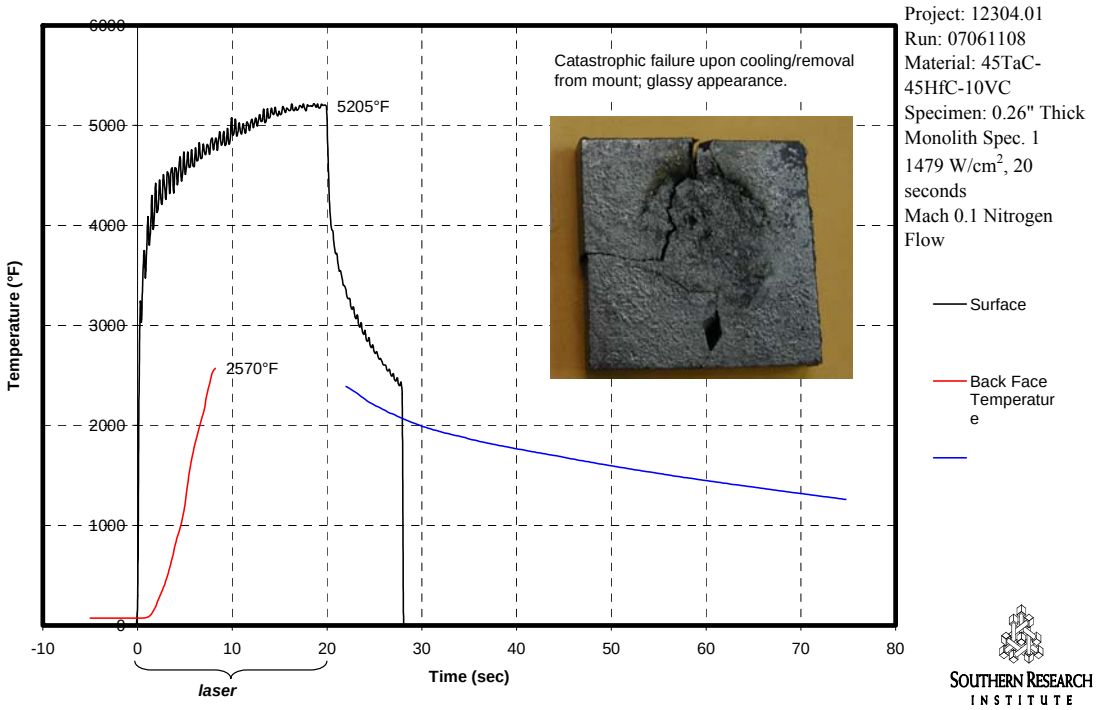

Thermal Response of 45TaC-45HfC-10VC at 1479 W/cm² in the LHMEL Facility

Figure A.2. Sample 07061109—Monolithic 45 wt% TaC- 45% HfC- 10% VC sample.

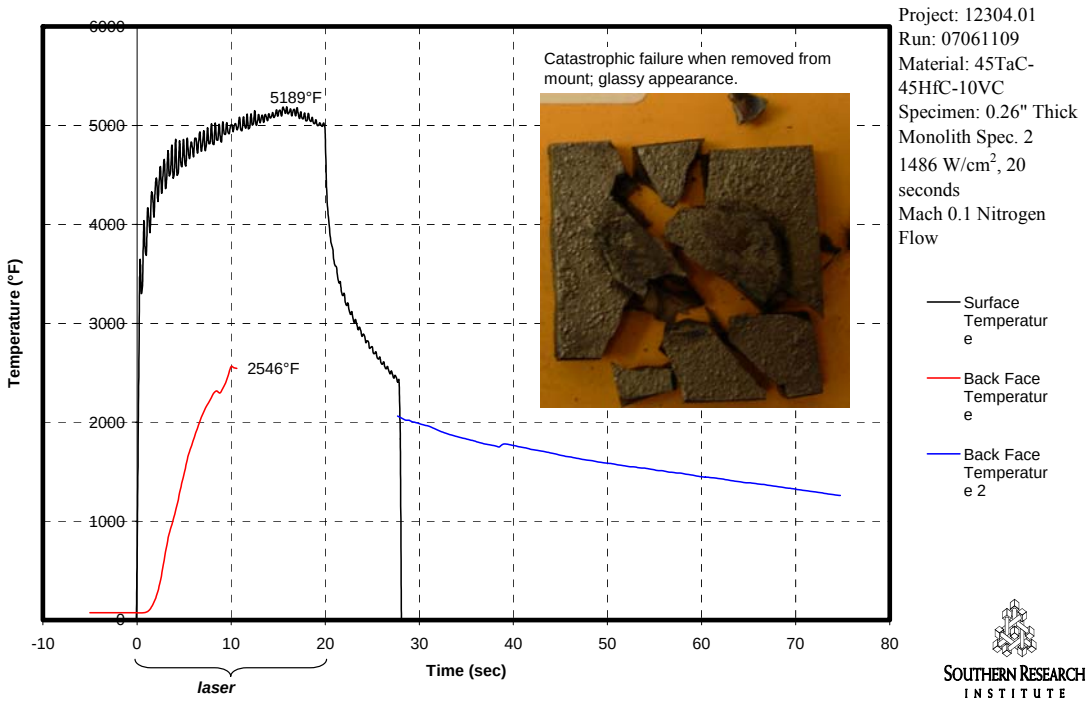

Thermal Response of 45TaC-45HfC-10VC at 1486 W/cm² in the LHMEL Facility

Microstructure of Monolithic 45 wt% TaC- 45% HfC- 10% VC: Sample #07061109

The fracture surface of the tested sample showed a bluish, yellowish dichromatic discoloration. Low magnification SEM analysis (Figure A.3) showed some dark spots, nominally 20 to 30 µm in size, scattered in a gray matrix. Higher magnification SEM of the matrix (Figure A.3) did not show features commonly observed on a fracture surface (i.e., angular features reminiscent of crack propagation through or around grains). It looked more like a thermal etched surface, partially revealing the grain boundaries. This might be caused by the laser heating associated with the test. An EDS spectrum (Figure A.4) suggests the composition of the matrix to be TaC, HfC, and VC. No oxygen or nitrogen was detected. Further analysis of the dark spots (Figure A.5) by EDS (Figure A.6) showed strong peaks for C, K, Na, and Cl, indicating some graphite and chloride based contamination was present in the starting materials.

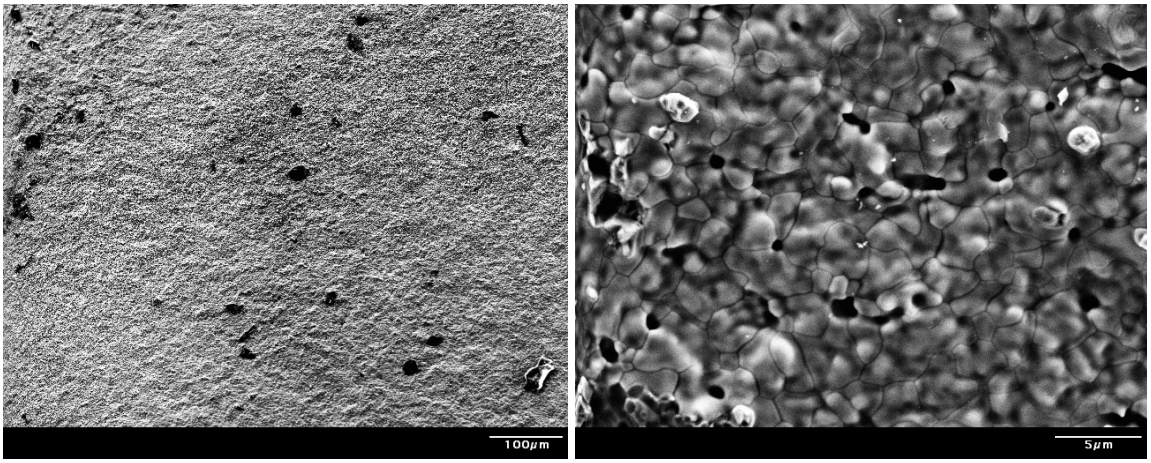

Figure A.3. SEM micrographs of the fracture surface of sample 07061109, monolithic 45 wt% TaC-45% HfC- 10% VC material.

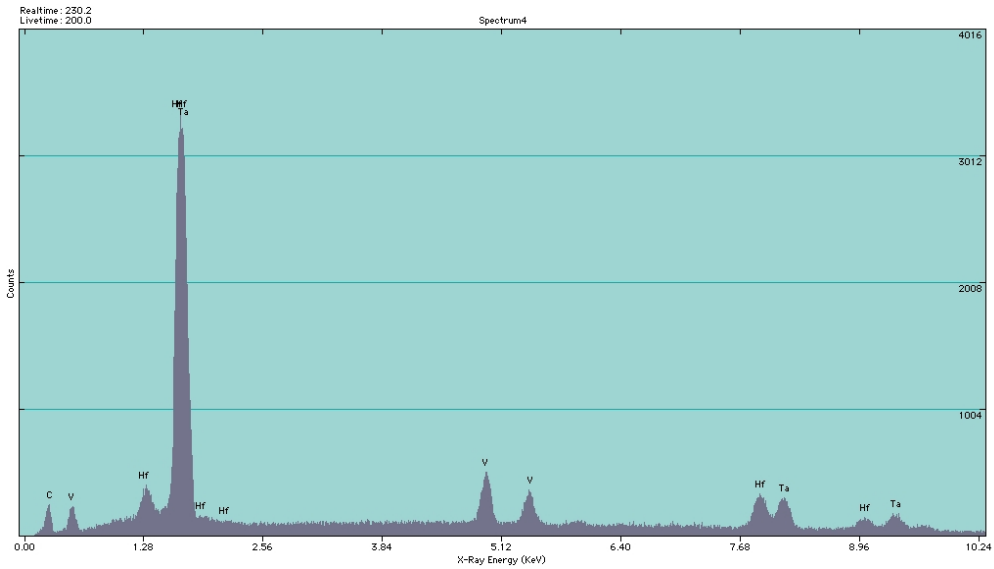

Figure A.4. EDS on fracture surface of sample 07061109, monolithic 45 wt% TaC- 45% HfC- 10% VC material.

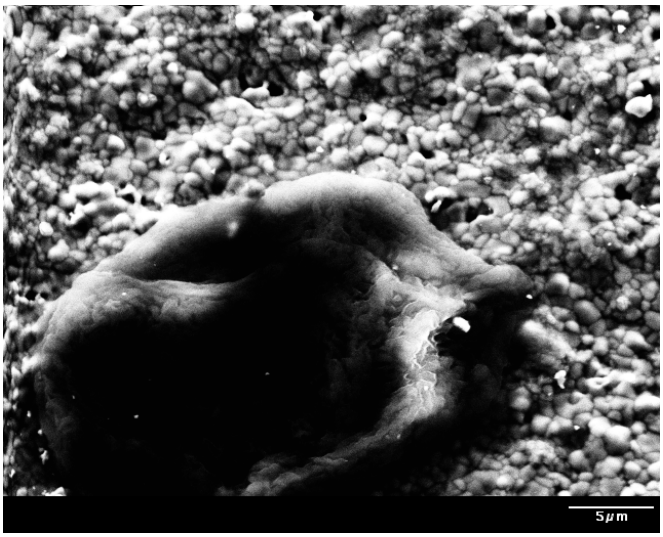

Figure A.5. Fracture surface of sample 07061109, monolithic 45 wt% TaC- 45% HfC- 10% VC, showing a dark piece

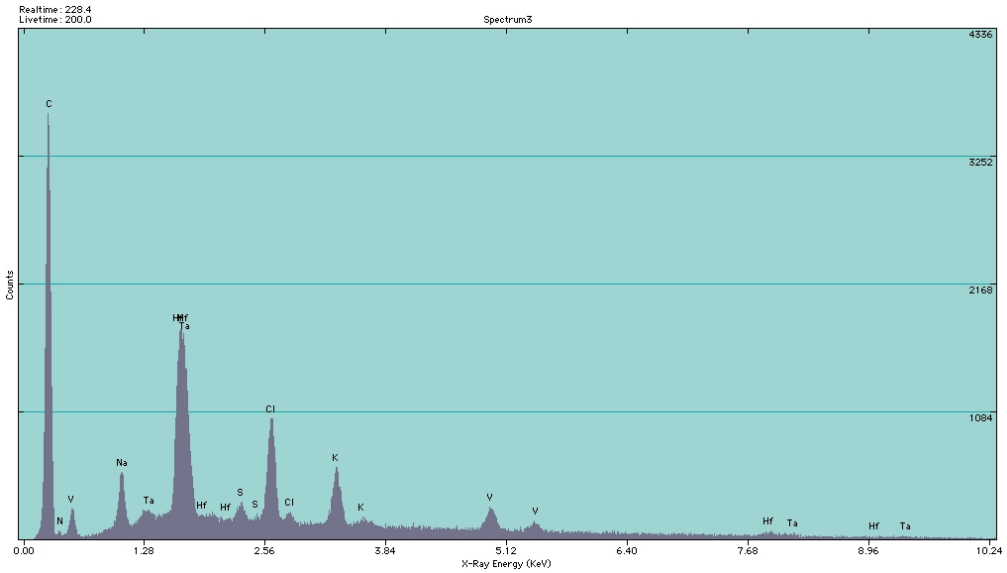

Figure A.6. EDS on the dark piece in Figure A.6

One piece of sample 07061109 was cut and polished (to 0.25 um surface finish) on the surface perpendicular to the LHMEL heated surface in an attempt to examine the bluish/yellowish surface discoloration. However, the microstructure (Figure A.7) did not show any discrete additional layer on the surface of the tested specimen.

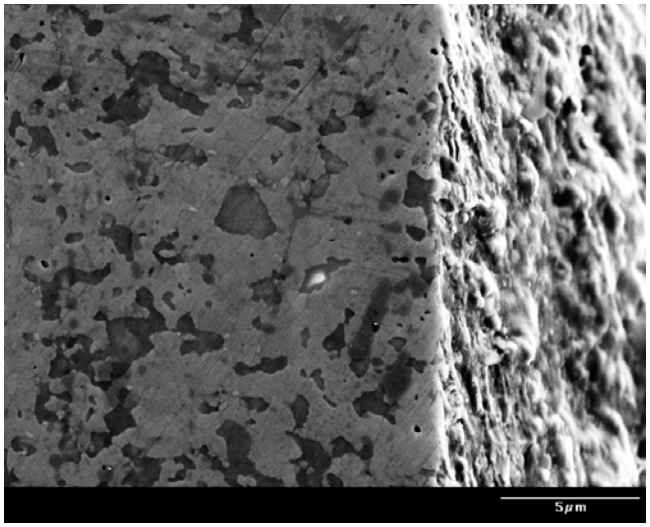

Figure A.7. SEM micrograph of polished cross section of sample 07061109, monolithic 45 wt% TaC- 45% HfC- 10% VC.

The glassy region of sample 07061109's exposed surface was also examined. The microstructure (Figure A.8) showed a dark continuous structure with bright grains segregated within the structure. EDS analysis was performed on dark and bright areas shown in the micrograph (Figure A.9). EDS on the dark layered structure revealed the presence of carbon, which is consistent with the appearance of the shiny surface. The bright grains were determined to be TaC, HfC, and VC.

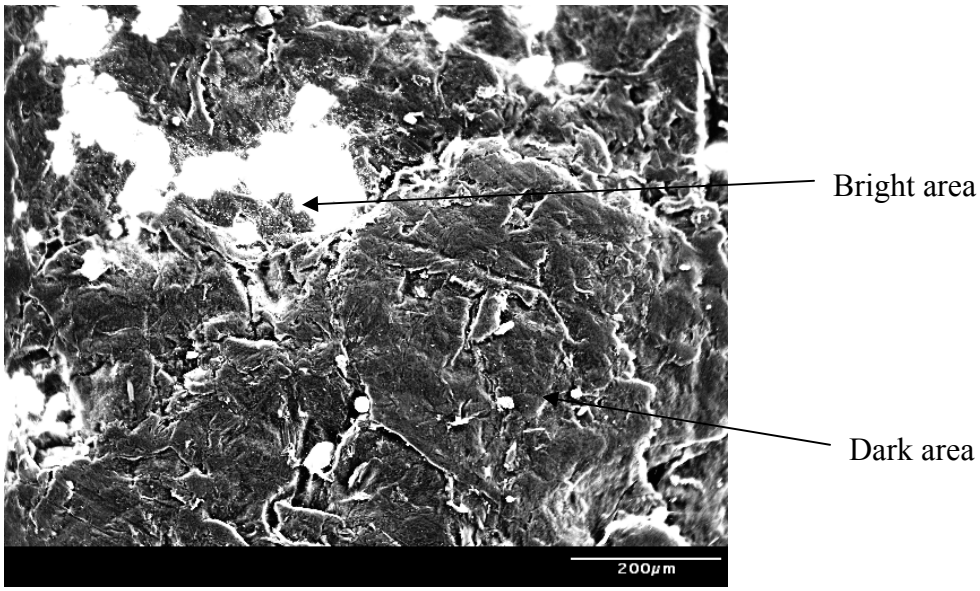

Figure A.8. SEM micrograph of glassy exposed region of sample 07061109, monolithic 45 wt% TaC- 45% HfC- 10% VC.

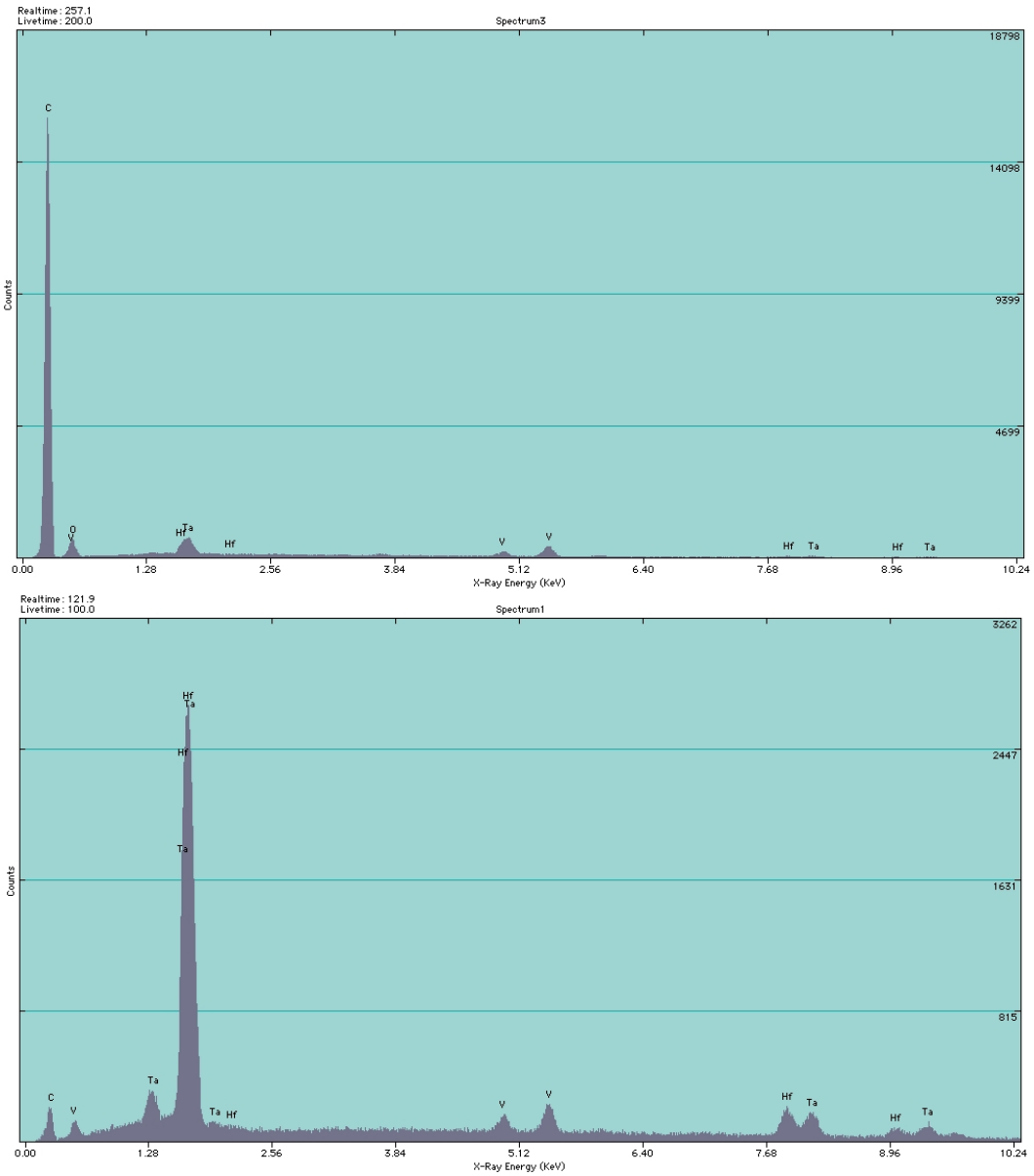

Figure A.9. EDS of dark area of glassy surface (top) and bright area (bottom) of sample 07061109, monolithic 45 wt% TaC- 45% HfC- 10% VC.

Figure A.10. Sample 07061107—Thin, uniaxial FM 45 wt% TaC- 45% HfC-10% VC sample.

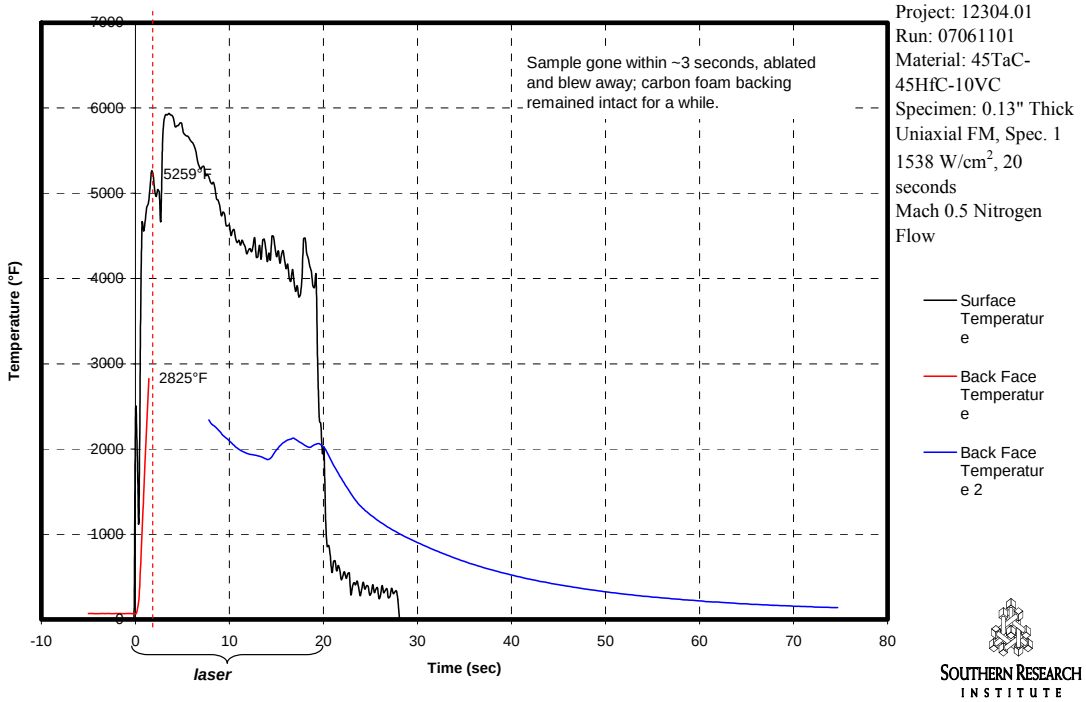

Figure 3.5.1-1 Thermal Response of 45TaC-45HfC-10VC at 1538 W/cm² in the LHMEL Facility

Figure A.11. Sample 07061115—Thin, uniaxial FM 45 wt% TaC- 45% HfC-10% VC sample.

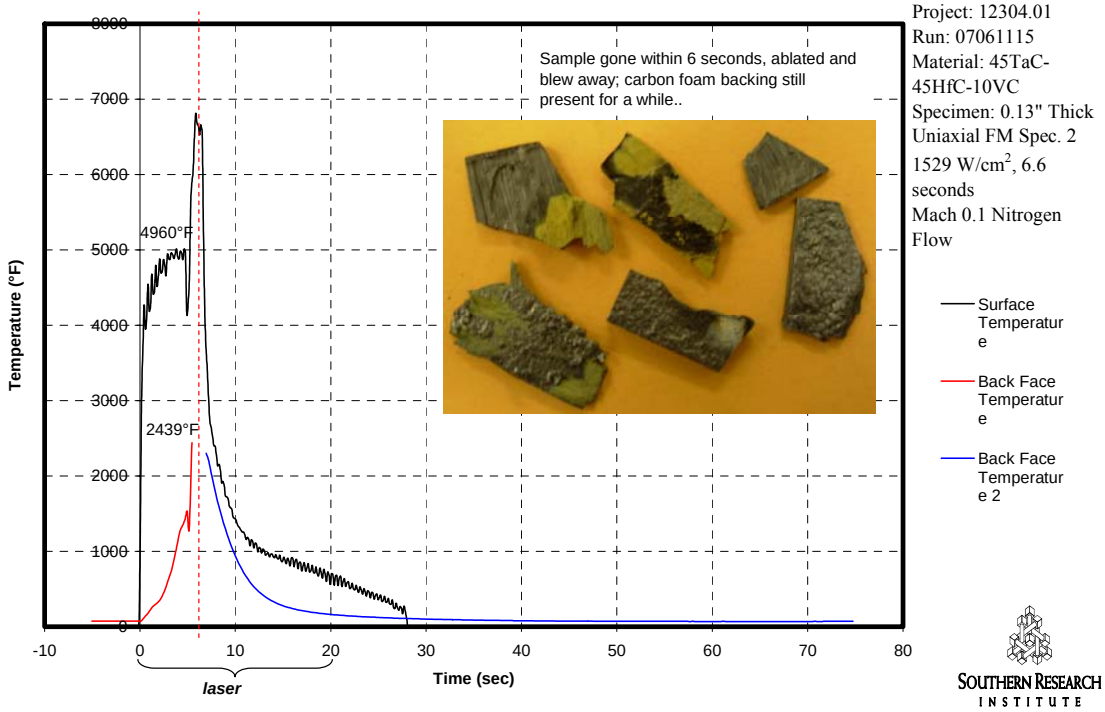

Thermal Response of 45TaC-45HfC-10VC at 1529 W/cm² in the LHMEL Facility

Microstructure of 45 wt% TaC- 45% HfC- 10% VC/ graphite Uniaxial FM: Sample # 07061115

Sample 07061115 failed early on during the test; samples were recovered downstream from the sample mount. The surface of the sample was yellow in color. Based on visual observations from the other tests, it is thought that this yellowing occurred during the sample's cooldown, once it had broken up and dropped out of the mount. The microstructure of the surface at low magnification (Figure A.12) shows the alignment of the filaments in the FM architecture. This fracture surface suggests failure occurred along the filaments. A look at the microstructure at higher magnification (Figure A.12) suggests that recrystallization may have occurred during the laser test. Large portions of the grains grew into a whisker-like shape, indicating the possibility that a phase transition has occurred in the system. TaC, HfC, and VC are all cubic in structure. Ta_2C and V_2C are hexagonal. We are hypothesizing that the carbides might have become carbon deficient during the test and transformed from cubic to hexagonal, causing the elongation of the grains. EDS analysis reveals that the whisker-shaped grains are still TaC, HfC, or VC (Figure A.13).

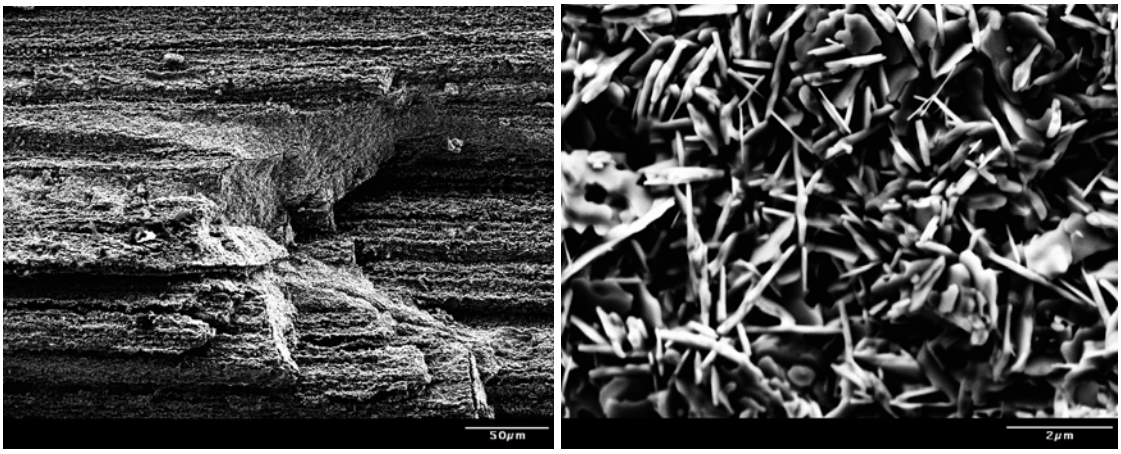

Figure A.12. SEM microstructure of the yellowed surface of sample 07061115, 45 wt% TaC- 45% HfC- 10% VC/graphite FM.

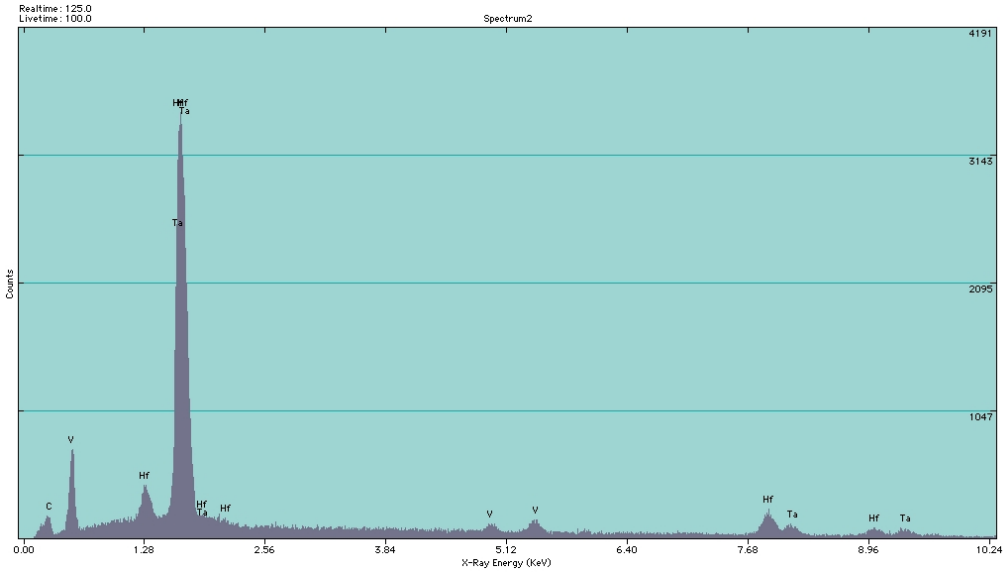

Figure A.13. EDS of yellowed whiskered surface of sample 07061115.

The fracture surface of sample 07061115 does not reveal the presence of the FM cell and cell boundary architecture (Figure A.14). Higher magnification imaging of the fracture surface (Figure A.14) shows a typical fracture pattern for a monolithic ceramic. EDS (Figure A.15) did not detect any other compound(s) except TaC, HfC, and VC. This result confirms the hypothesis that the graphite shell material is consumed during the exposure.

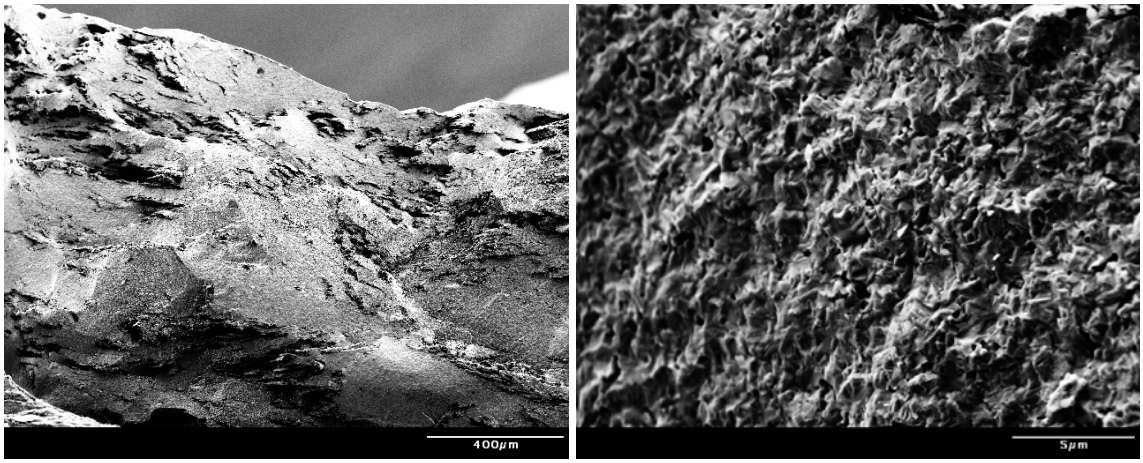

Figure A.14. Fracture surface of sample 07061115, 45 wt% TaC- 45% HfC- 10% VC/ graphite FM.

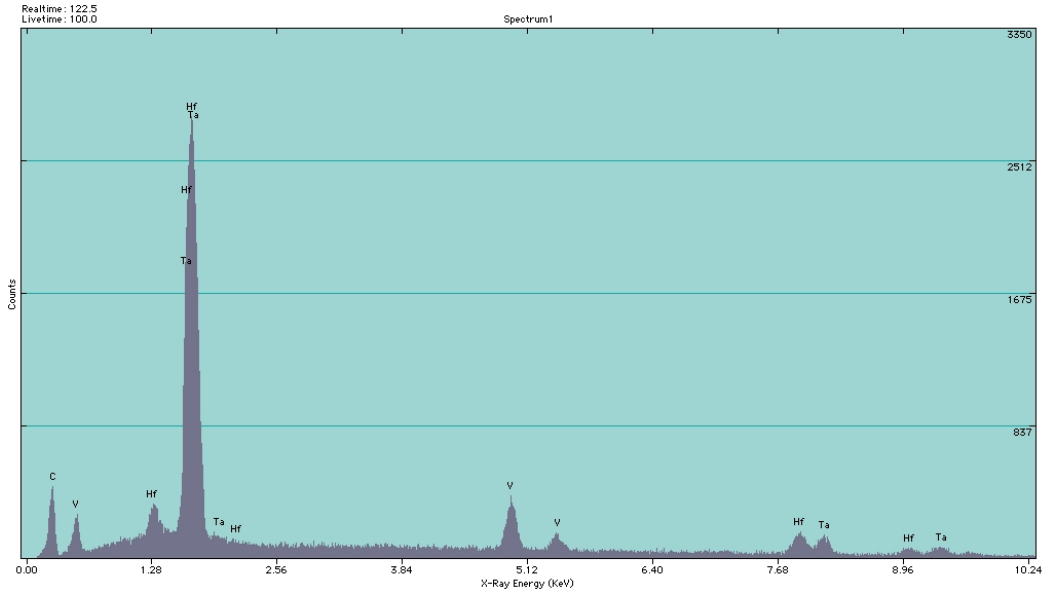

Figure A.15. EDS on the fracture surface of sample 07061115, 45 wt% TaC- 45% HfC- 10% VC/ graphite FM.

The yellow surface of sample 07061115 was analyzed by XRD to determine the composition. The XRD pattern (Figure A.16) shows the presence of two oxides—Ta_2O_5 and $Hf_6Ta_2O_{17}$—on the surface with $Hf_6Ta_2O_{17}$ dominating. Yellowing of the samples tested was observable only when a heated sample was cooled down in the presence of oxygen, suggesting that the oxides most likely formed after the sample broke away from the mount, during the cooling from peak temperature. The formation of Ta_2O_5 and HfO_2 are both favorable at room temperature. The formation of $Hf_6Ta_2O_{17}$ might have occurred as Reaction (1). An attempt was made to calculate the thermodynamic favorability of this reaction using a commercial software program (HSC Chemistry, Fairfield, California, USA), but no thermodynamic data was found for $Hf_6Ta_2O_{17}$. Other resources such as JANAF table and database in FactSage also do not include this compound.

$$Ta_2O_5 + 6HfO_2 = Hf_6Ta_2O_{17} \qquad (1)$$

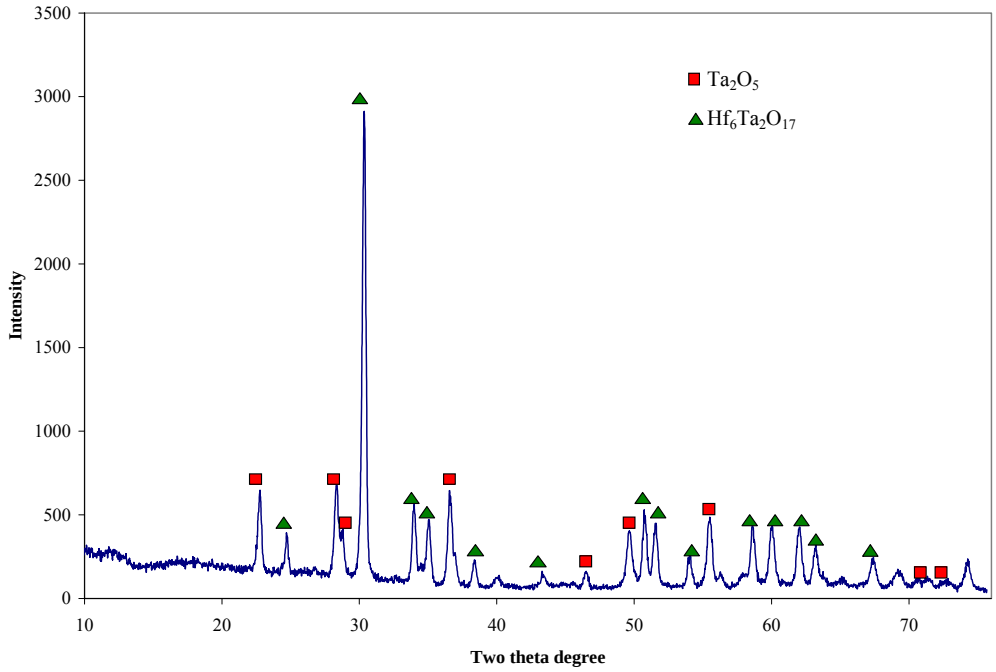

Figure A.16. XRD pattern of the yellow surface of sample 07061115, monolithic 45 wt% TaC- 45% HfC- 10% VC.

Figure A.17. Sample 07061110—Thick, uniaxial FM 45 wt% TaC- 45% HfC- 10% VC sample.

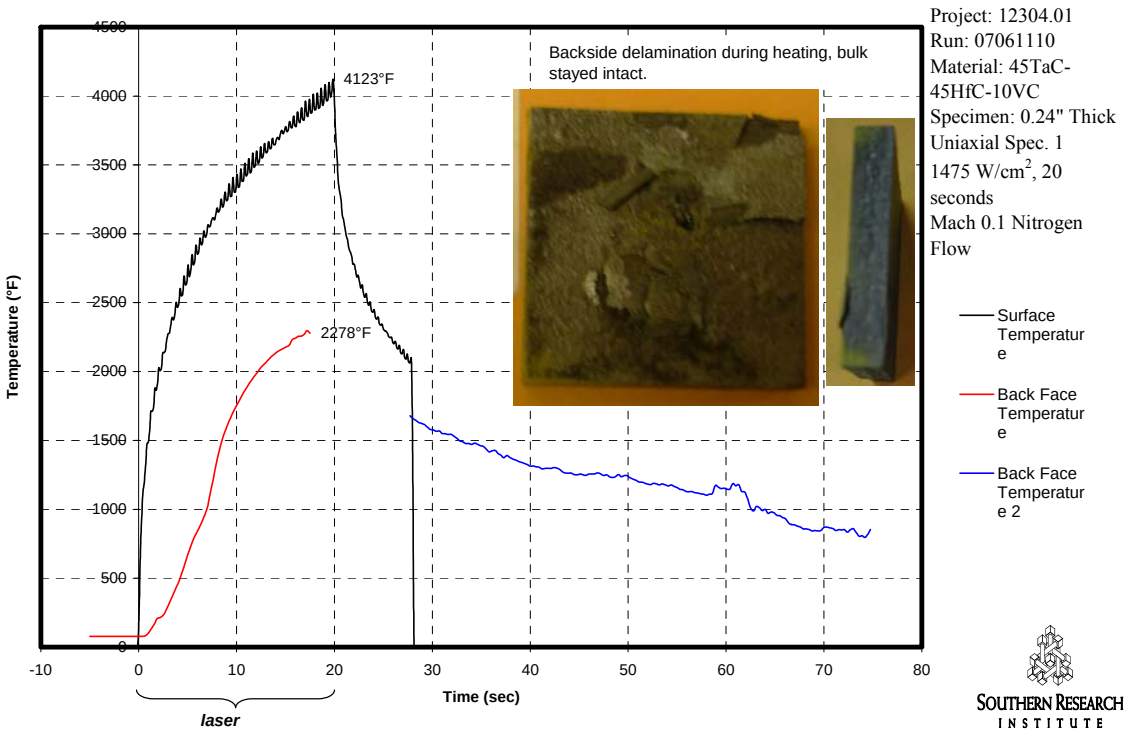

Thermal Response of 45TaC-45HfC-10VC at 1475 W/cm² in the LHMEL Facility

Figure A.18. Sample 07061111—Thick, uniaxial FM 45 wt% TaC- 45% HfC- 10% VC sample.

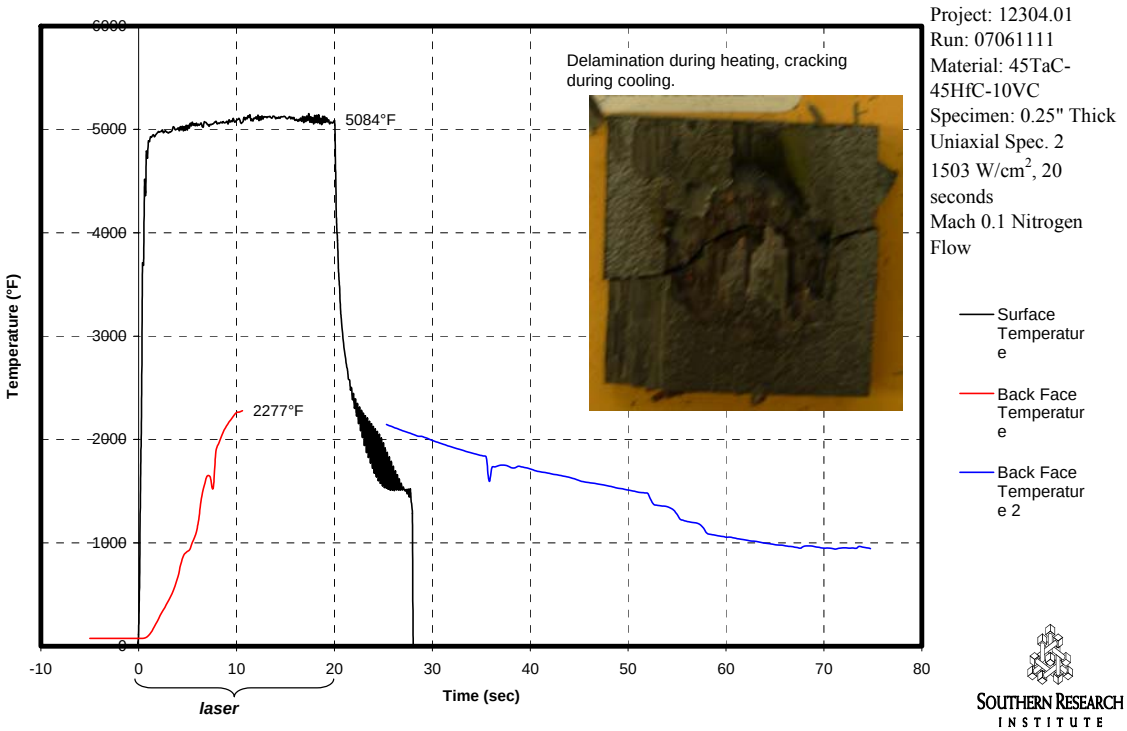

Thermal Response of 45TaC-45HfC-10VC at 1503 W/cm² in the LHMEL Facility

Monolithic and Fibrous Monolithic 75 vol% TaC- 20% HfC- 5% VC Material Evaluation

Figures A.19 through A.33 illustrate exposed monolithic and fibrous monolithic materials constructed using the TaC-rich blend developed during the Phase II program.

Figure A.19. Sample 07061102—Monolithic 75 vol% TaC- 20% HfC- 5% VC sample.

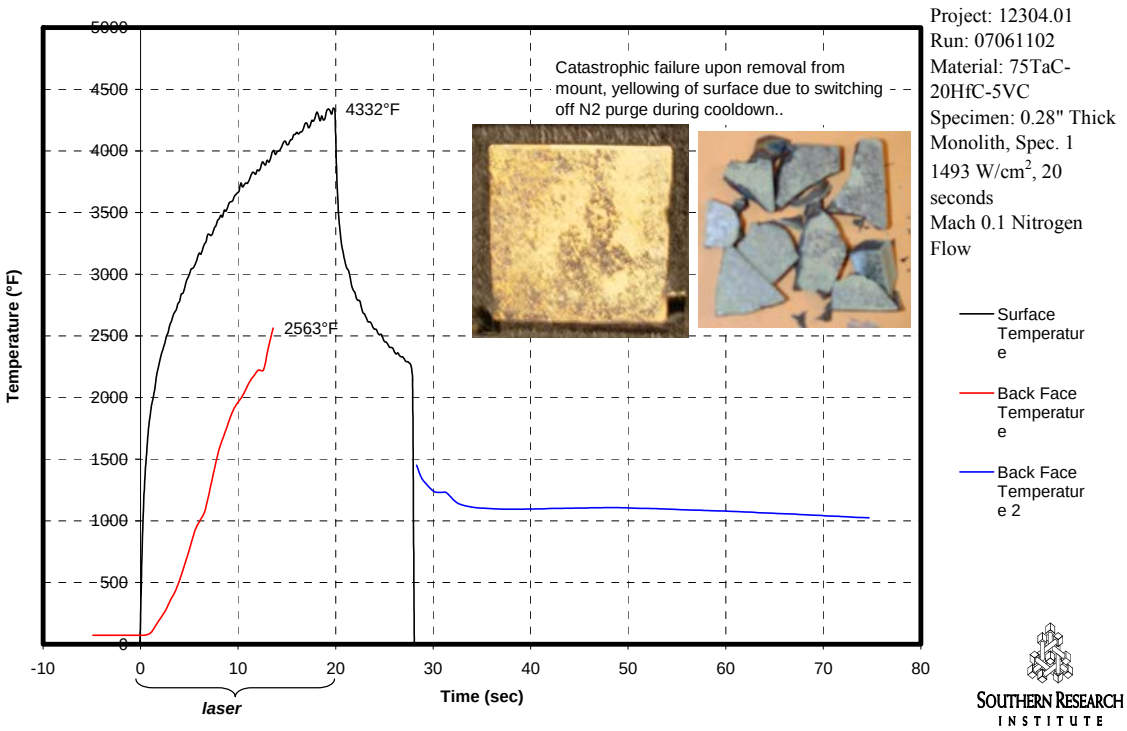

Thermal Response of 75TaC-20HfC-5VC at 1493 W/cm² in the LHMEL Facility

Figure A.20. Sample 07061113—Thin, uniaxial FM 75 vol% TaC- 20% HfC- 5% VC sample.

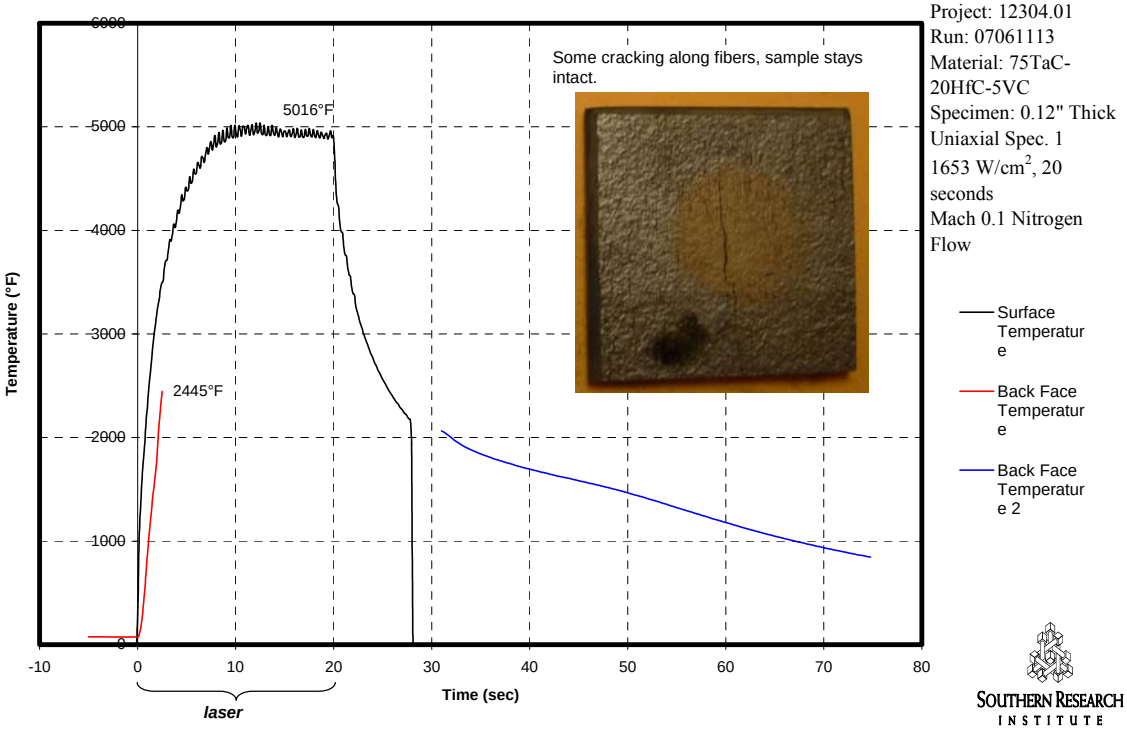

Thermal Response of 75TaC-20HfC-5VC at 1653 W/cm² in the LHMEL Facility

Figure A.21. Sample 07061114—Thin, uniaxial FM 75 vol% TaC- 20% HfC- 5% VC sample.

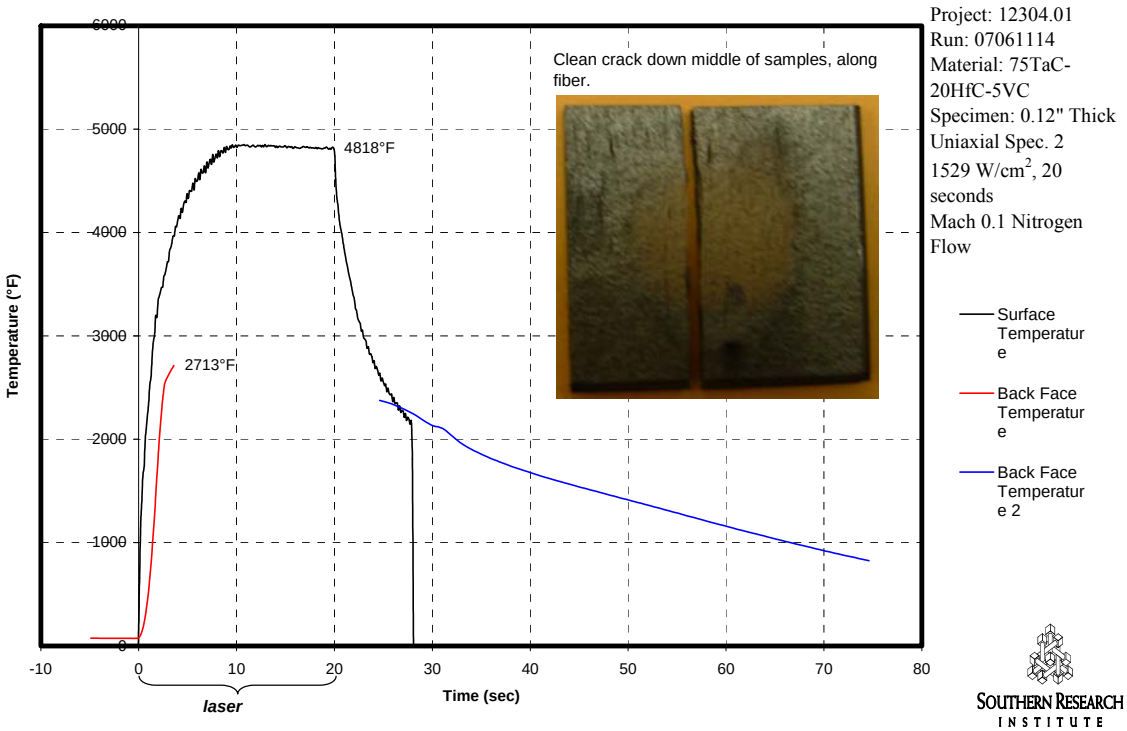

Thermal Response of 75TaC-20HfC-5VC at 1529 W/cm² in the LHMEL Facility

Microstructure of 75 vol% TaC- 20% HfC- 5% VC/graphite Uniaxial FM: Sample # 07061114

Figure A.21 shows a slight discoloration of the irradiated area of sample 07061114; this region was examined using SEM. Figure A.22 was obtained from the copper colored irradiated area. The center of the exposed region appears to be more porous than the surrounding area. EDS analysis performed on the center region showed that it was composed of TaC, HfC, and VC (Figure A.23). There was no evidence of oxide formation on the surface.

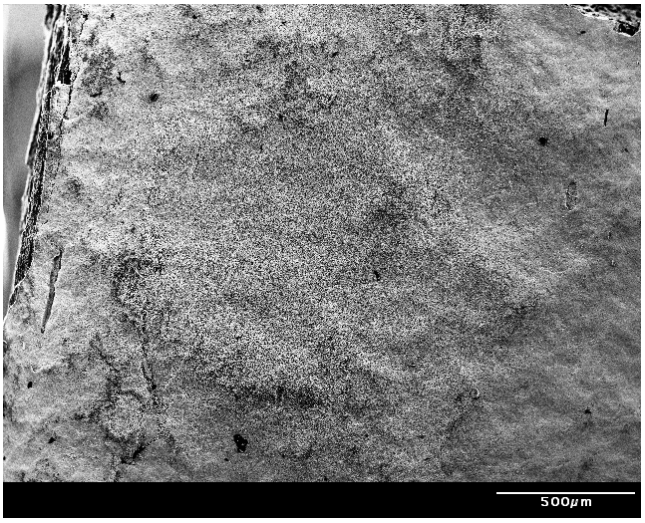

Figure A.22. Center of irradiated region on surface of sample 07061114, 75 vol% TaC- 20% HfC- 5% VC/ graphite FM.

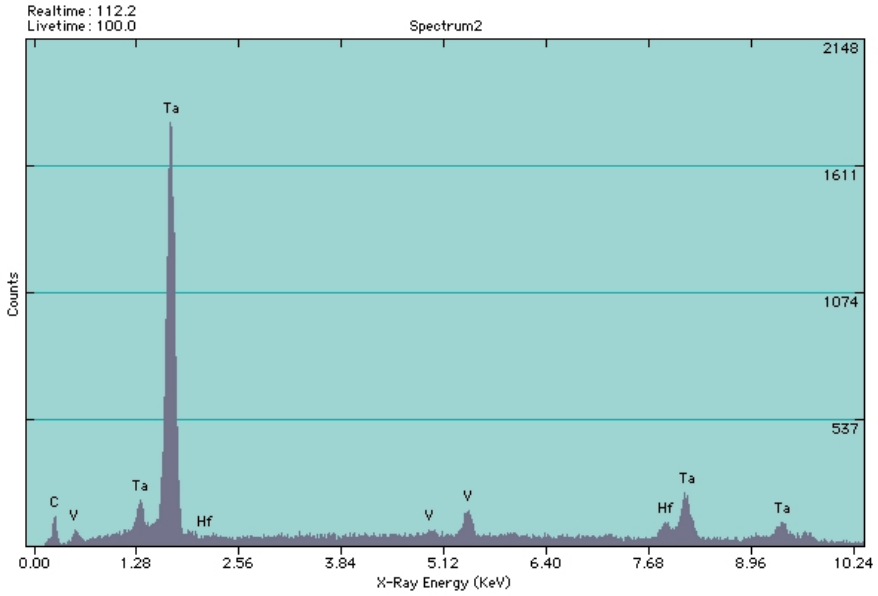

Figure A.23. EDS of center of irradiated region of sample 07061114.

Images were also taken away from the center of the irradiated region. Black patches observable throughout the grey matrix in the SEM micrograph shown in Figure A.24 have been identified as carbon by EDS analysis (Figure A.25). Figure A.26 shows micrographs of the 07061114 sample surface from the center to the outer edge of the exposed region. The third SEM micrograph shown in Figure A.26, obtained from the edge of visibly discolored irradiated region, shows some features of the fibers and more concentrated black patches. The increasing number of graphitic patches as you move farther away from the center of irradiation indicates that the graphitic shell phase is selectively removed during exposure.

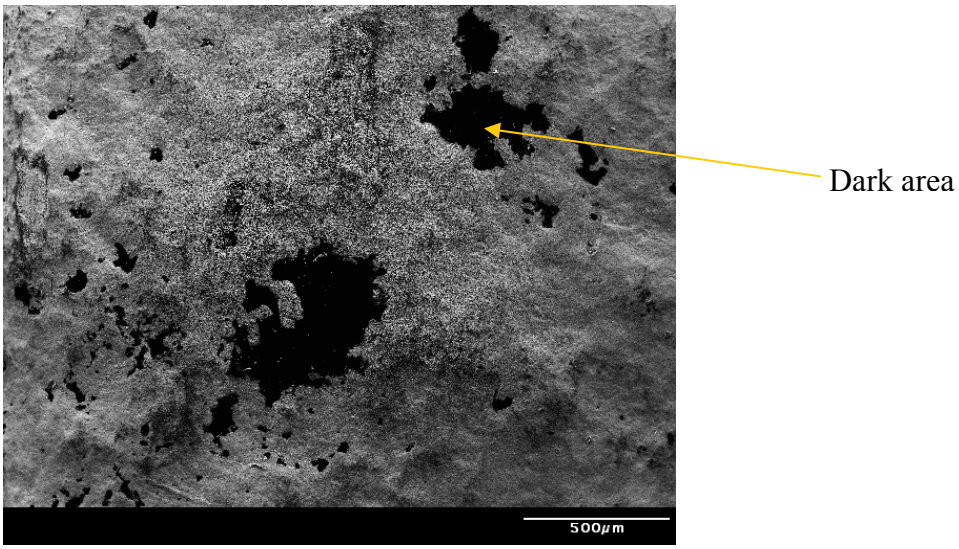

Figure A.24. SEM micrograph of the surface of sample 07061114 taken slightly away from the center of irradiated region.

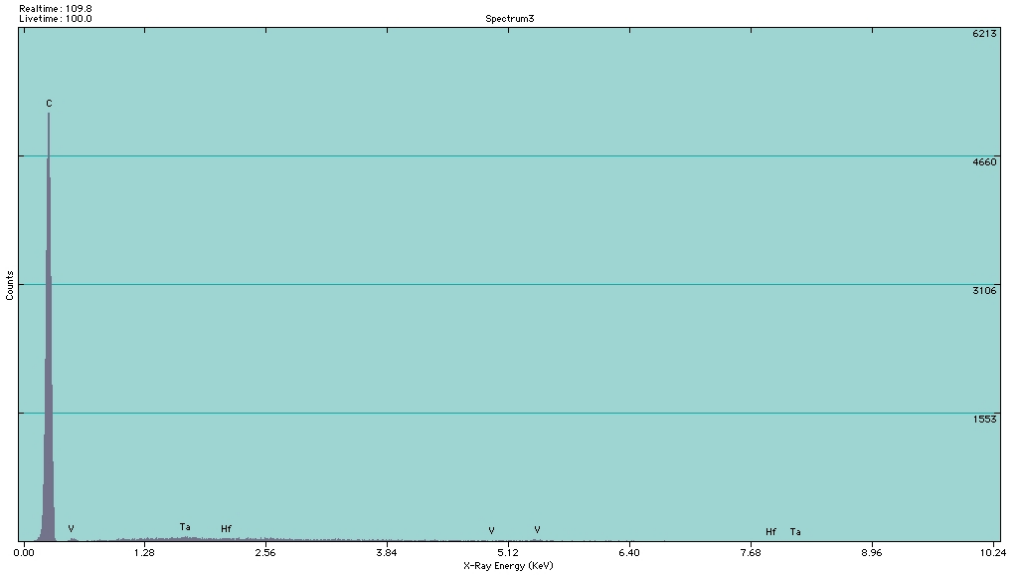

Figure A.25. EDS of dark area of sample 07061114 shown in Figure A.24

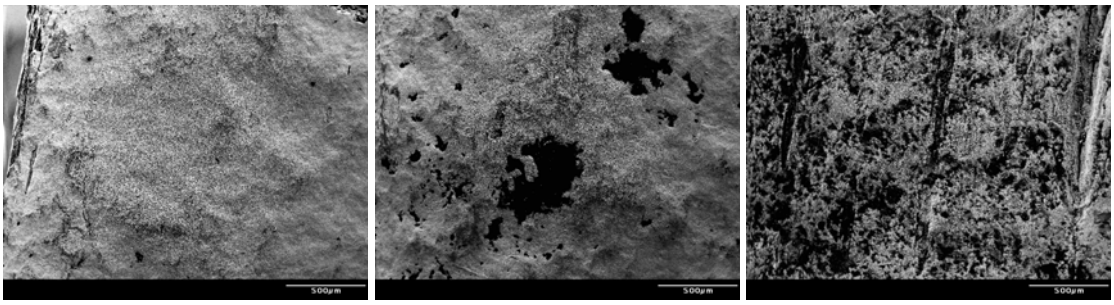

Figure A.26. SEM micrograph of exposed surface of sample 07061114—Images of exposed region (left), slightly away from center of the exposure (middle), and along the edge of the irradiated region (right).

The cross section of the irradiated region shown in Figure A.27 reveals the macrostructure of the FM architecture. The cells do not appear to be fully dense.

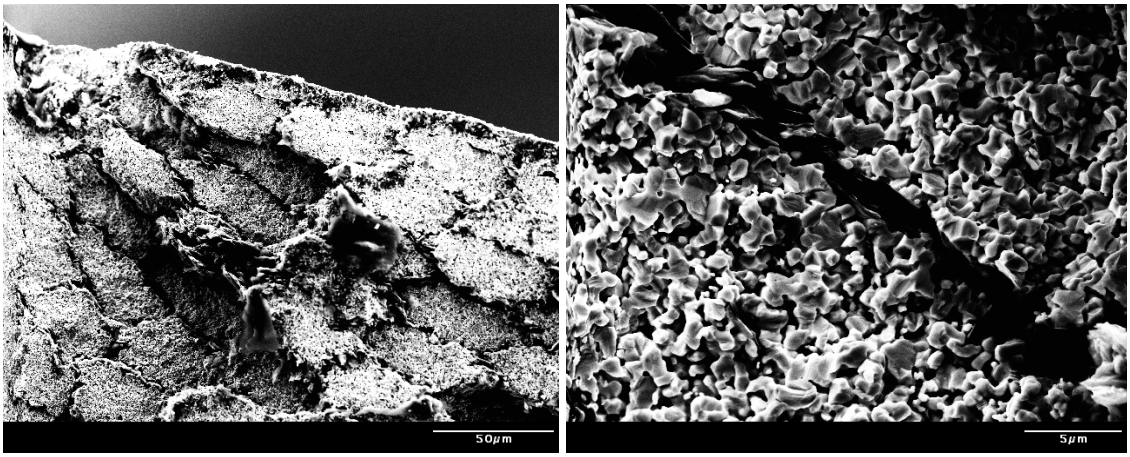

Figure A.27. Cross sectional SEM micrograph of sample 07061114, 75 vol% TaC- 20% HfC- 5% VC/ graphite FM.

Figure A.28. Sample 07061103—Thick, uniaxial FM 75 vol% TaC- 20% HfC- 5% VC sample.

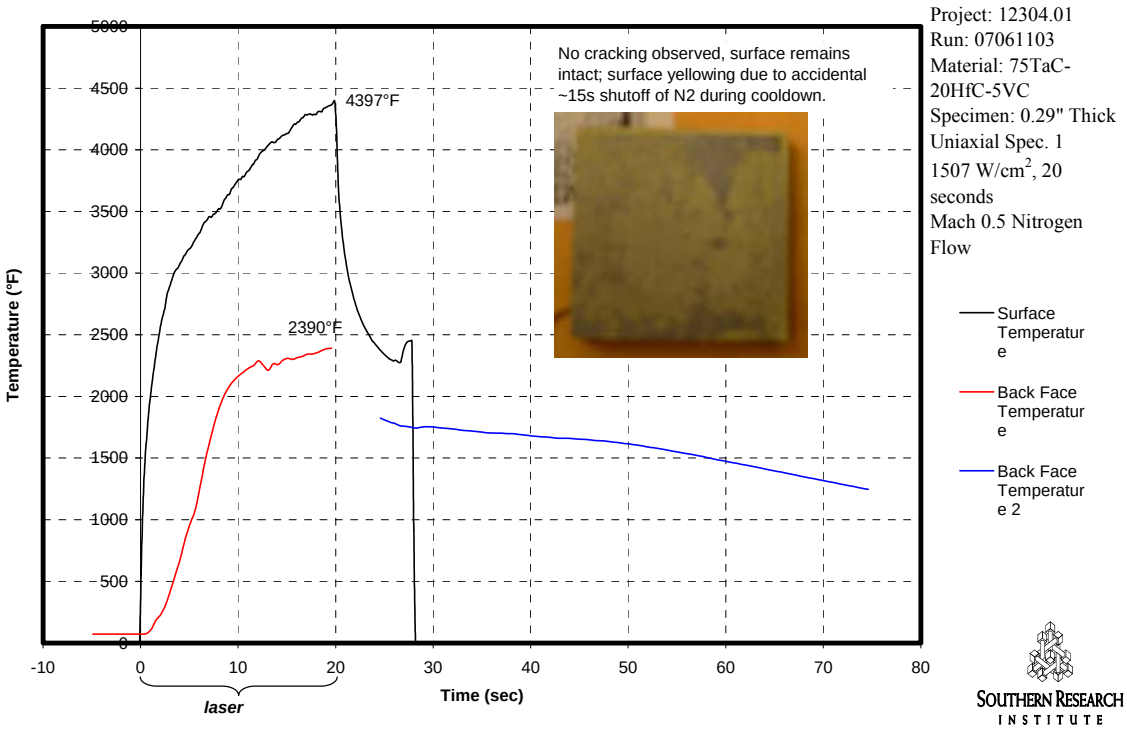

Thermal Response of 75TaC-20HfC-5VC at 1507 W/cm² in the LHMEL Facility

Figure A.29. Sample 07061105—Thick, uniaxial FM 75 vol% TaC- 20% HfC- 5% VC sample.

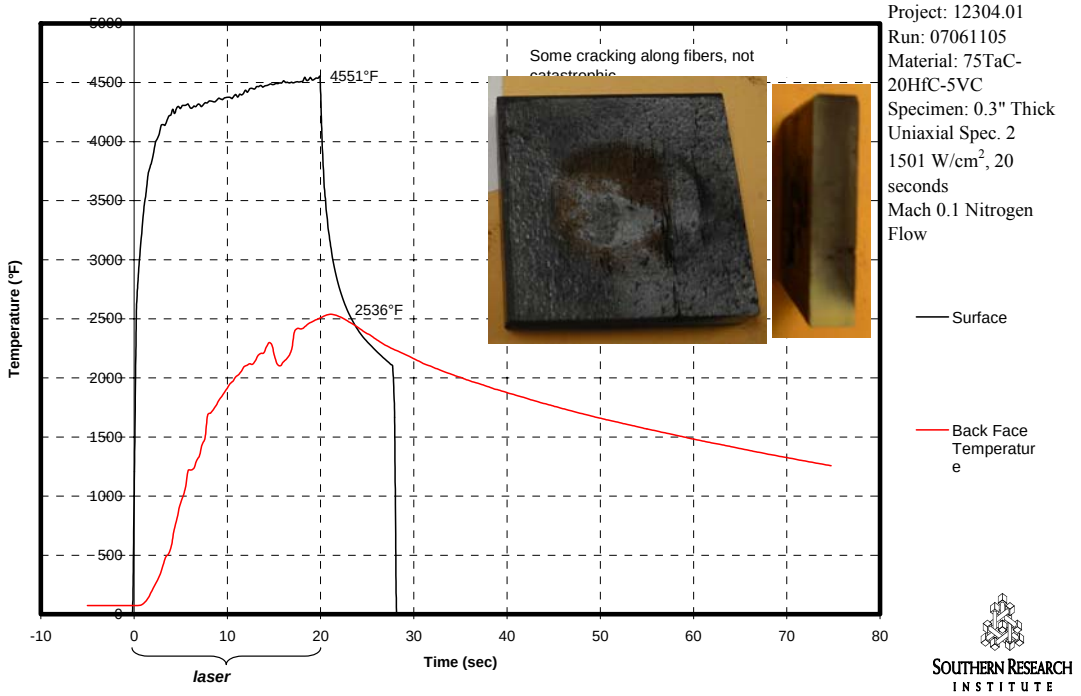

Thermal Response of 75TaC-20HfC-5VC at 1501 W/cm² in the LHMEL Facility

Figure A.30. Sample 07061104—Thin, biaxial FM 75 vol% TaC- 20% HfC- 5% VC sample.

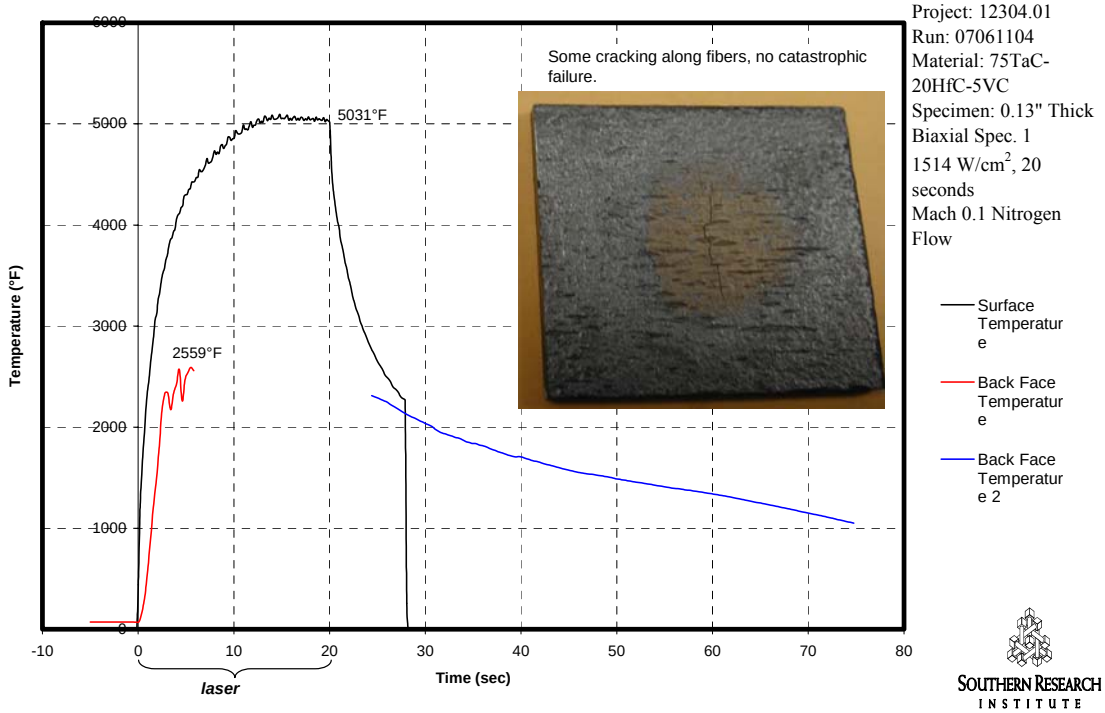

Thermal Response of 75TaC-20HfC-5VC at 1514 W/cm² in the LHMEL Facility

Figure A.31. Sample 07061112—Thin, biaxial FM 75 vol% TaC- 20% HfC- 5% VC sample.

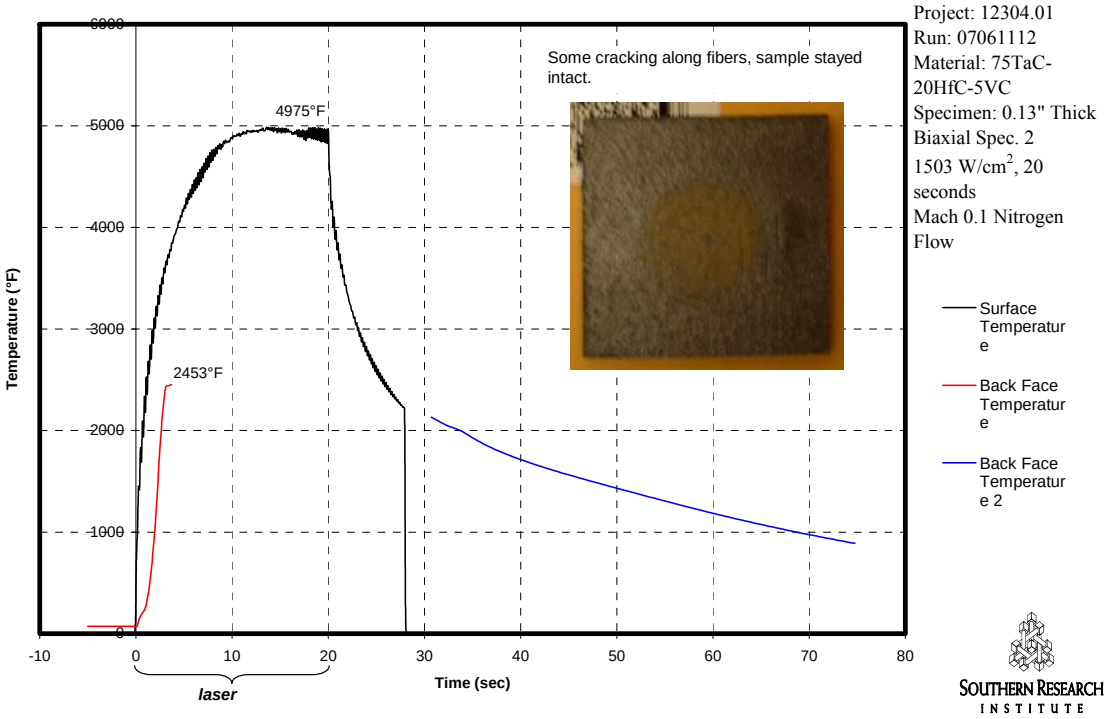

Thermal Response of 75TaC-20HfC-5VC at 1503 W/cm² in the LHMEL Facility

Figure A.32. Sample 07061106—Thick, biaxial FM 75 vol% TaC- 20% HfC- 5% VC sample.

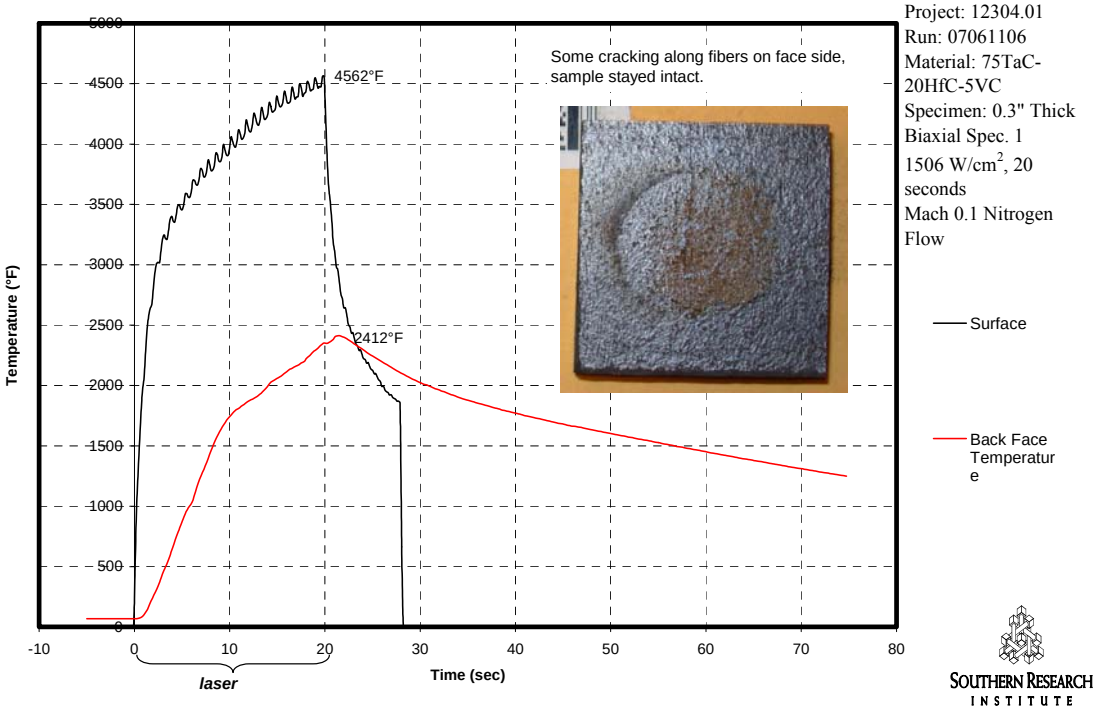

Thermal Response of 75TaC-20HfC-5VC at 1506 W/cm² in the LHMEL Facility

Figure A.33. Sample 07061107—Thick, biaxial FM 75 vol% TaC- 20% HfC- 5% VC sample.

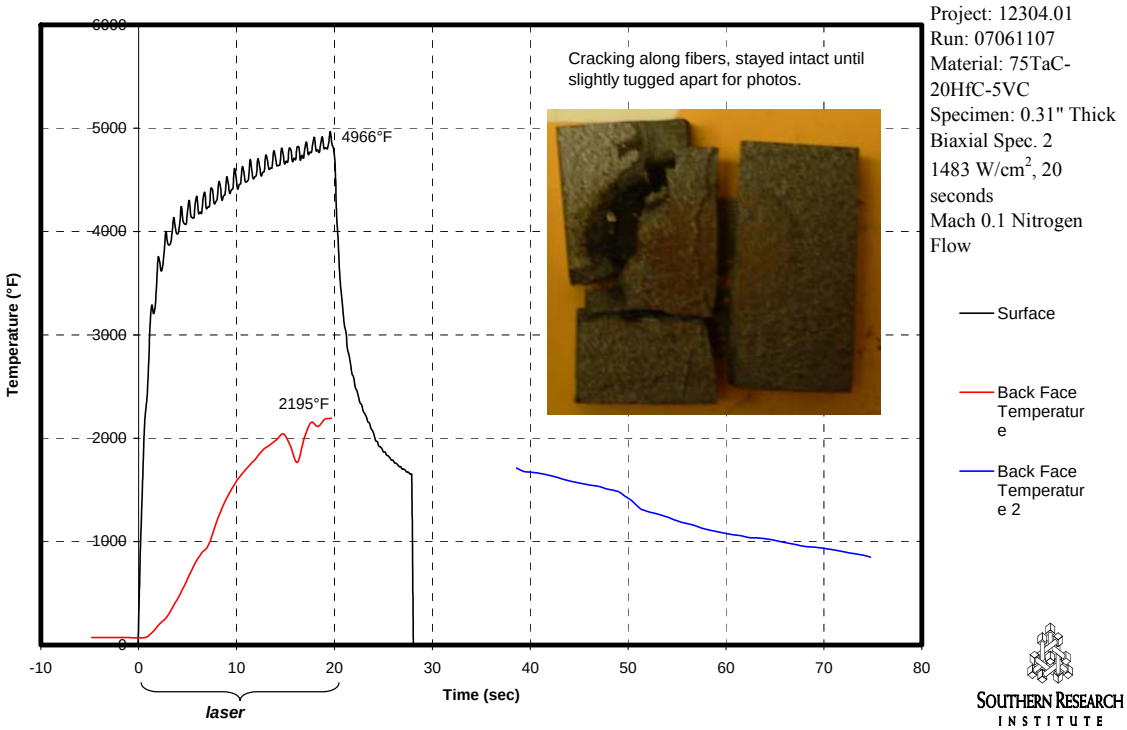

Thermal Response of 75TaC-20HfC-5VC at 1483 W/cm² in the LHMEL Facility

Appendix B: Evaluation of Grain Growth Controlling Additions by UMR

Hot Pressing of TaC With and Without Sintering Additives—TaC with B_4C and C

Densification of TaC, with and without sintering additives, was studied at processing temperatures ranging from 1900 to 2400ºC. Without sintering additives, the relative density increased from 75% at 1900ºC to 96% at 2400ºC. A microstructural examination showed no observable grain growth up to 2300ºC. Grain growth became significant above 2300ºC, resulting in a limited final density. Densification was enhanced with carbon (C) and/or boron carbide (B_4C) additions which assisted in the removal of oxide impurities on the surface of the starting TaC powder. TaC with 0.78 wt% C additions achieved a relative density of 97% at 2300ºC. Grain growth initiated at this temperature and resulted in partly entrapped and partly open porosity. TaC with 0.36 wt.% B_4C additions achieved relative densities of 98% at 2200ºC, with grain growth becoming rapid at 2150ºC and higher temperatures. TaC with 0.43 wt% B_4C + 0.13 wt% C additions resulted in relative densities of 98% at 2200ºC, again accompanied by rapid grain growth at 2100ºC and higher temperatures.

Summary

Tantalum carbide (TaC) powder was hot pressed, with and without additional sintering additives, in the temperature range of 1900-2400ºC. In view of the difficulty densifying pure TaC, sintering additives such as carbon (C) and/or boron carbide (B_4C) have been selected to enhance densification. The onset temperature of densification was significantly lowered with the addition of sintering additives, although grain growth was consequently initiated at lower temperatures.

Introduction

Because of its high melting point (3983ºC), high hardness, and resistance to chemical attack and oxidation, TaC is regarded as a potential structural material in extremely high temperature applications such as rocket nozzles and jet engine components. Unfortunately, monolithic TaC is difficult to densify even with the application of external pressing (hot pressing) due to its highly covalent bonding character and low self-diffusion coefficient. Samsonov, et.al[2] determined the activation energy for viscous flow of various carbides and found the activation energy for sintering of TaC to be 97 kcal/mol, the highest among the various carbides. In order to promote densification, ultra fine starting powders[3,4], high pressure[3], mixed carbides[5], and liquid phase sintering[6,7] have been investigated in the literature. Even with ultrafine powders, full density was not obtained consistently because of impurities, such as surface oxides, in the starting powders. Transition metals such as Mn, Co, Ni, and Fe have been used to liquid phase sinter TaC. The sintering temperatures were lowered with the additions of transition metals. However, the presence of liquid phase caused rapid grain growth ultimately leading to lower densities and strengths. Further, the presence of metallic phases at the

grain boundaries is known to limit the usefulness of ceramics for high-temperature applications[8].

The presence of oxide impurities on the surface of particles has been blamed for inhibiting sintering in many non-oxide ceramics such as TiB_2[9], SiC[10], B_4C[11], and ZrB_2[12, 13]. Reactive additives, such as C and B_4C, have been used to remove oxides in SiC, B_4C, and ZrB_2 to promote densification. However, the additions of sintering additives such as C and B_4C to enhance the densification of TaC have not been reported in the literature. Therefore, the objective of this work is to study the densification of monolithic TaC and to evaluate the effect of C and B_4C additions on densification. A commercial software program (HSC Chemistry, Fairfield, CA, USA) was used to calculate the change in Gibbs free energy for the reduction of Ta_2O_5 (the surface oxide expected to on the TaC powder) with several potential reducing agents. The reduction of Ta_2O_5 by either C and/or B_4C proceeds according to Reactions (1) to (3). The development of microstructures with and without sintering additives will be examined and related to the processing parameters. In addition, the mechanical properties of TaC are sparse throughout the literature dating back to the 1960's. Therefore, mechanical properties such as elastic modulus, bending strength, fracture toughness, and microhardness of the densified TaC materials will be tested.

$$Ta_2O_5 + 7C = 2TaC + 5CO \quad (1)$$
$$\Delta G^0_{rxn1} = -18164J \text{ at } 1200^oC$$

$$1.4Ta_2O_5 + B_4C = 2.8Ta + 2B_2O_3(l) + CO \quad (2)$$
$$\Delta G^0_{rxn2} = -23509J \text{ at } 1100^oC$$

$$1.2Ta_2O_5 + B_4C + 1.4C = 2.4TaC + 2B_2O_3 \quad (3)$$
$$\Delta G^0_{rxn3} = -373166J \text{ at } 0^oC$$

Experimental Procedure

Raw materials

TaC and B_4C powders, along with phenolic resin, were the starting raw materials for this study. The grade, particle size, surface area, and suppliers are listed, where appropriate, for the raw materials in Table B.1. The average particle size of the TaC powder was measured to be 2.4 μm. The particle size of the B_4C was quoted by the supplier. The surface area of TaC and B_4C powders were measured using nitrogen absorption (NOVA 1000, Quantachrome, Boynton Beach, FL). The morphology of the TaC powder was examined using scanning electron microscopy (SEM Hitachi S570, Hitachi, Tokyo, Japan) and is shown in Figure B.1. The powder exhibited bi-modal particle size distribution.

Table B.1. Raw Material Characteristics

Material	Grade	Particle size (μm)	Surface area (m^2/g)	Supplier
TaC	TA-301	2.4	1.5	Atlantic Equipment Engineers
B_4C	HS	0.8	15.8	H.C. Starck
Phenolic resin		flakes		Georgia Pacific

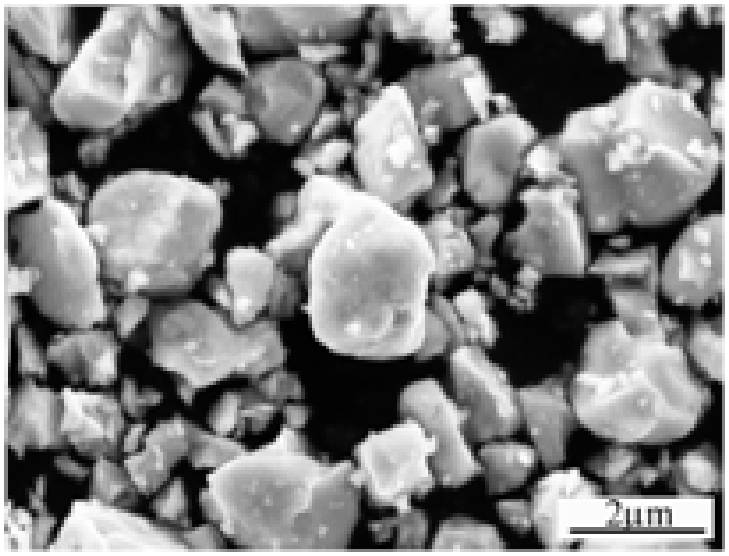

Figure B.1. SEM image of the as-received TaC powder.

Mixing of TaC powder and sintering additives

Phenolic resin is being used as a carbon precursor. The process currently being used in this study has been illustrated in the form of a flowchart (Figure B.2). The phenolic resin is dissolved in acetone to which TaC powder (and B_4C powder) is added. The slurry is then ultrasonically mixed for 15 min prior to rotary evaporation (Rotavapor R-124, Bucchi, Flawil, Germany) to remove the acetone at a temperature of 70ºC, vacuum of -25 mmHg, and a rotation speed of 130 rpm. The powders are then charred under a stagnant vacuum at 450°C for 2 hours to produce carbon, followed by grinding and sieving (200 mesh, <74 microns) to produce the final powders for hot pressing.

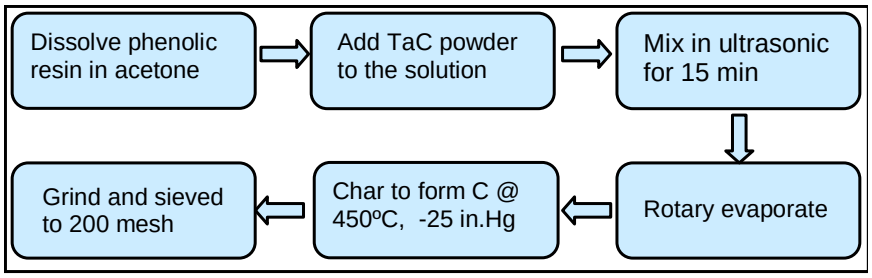

Figure B.2. Flowchart for processing with carbon additions.

Hot pressing and characterization

TaC powder with and without additives were hot pressed in a graphite die using a graphite resistance hot press (Astro HP-20-3060, Thermal Technology, Santa Rosa, CA) over a range of temperatures (1900-2400ºC) and at an applied pressure of 30 MPa for a hold of 45 min at the final hot pressing temperature. The powder compact was heated up at 5ºC/min under vacuum to 1200ºC and with a hold of 1 hour to allow the reduction reaction to complete. The temperature was then increased to 1450ºC and with a hold of 1 hour, allowing the samples to outgas. Another 1 hour hold was added at 1650ºC for additional outgassing, after which either flowing argon (≤2100ºC) or helium (>2100ºC) was introduced into the furnace. The pressure was gradually applied at 100ºC below the desired hot pressing temperature. The pressure and desired temperature were reached simultaneously. After a 45 min hold at the desired temperature, the sample was cooled slowly to room temperature.

The hot pressed samples were surface ground and cut along the hot pressing direction. The relative density was measured using the Archimedes method. The cross section was polished with diamond abrasive successively to 0.25 μm before being thermally etched at 1650ºC for 1 hour. The microstructure of the thermal etched samples was then examined using SEM.

Results and Discussion

Densification of TaC without sintering additives

The relative densities versus hot pressing temperature for as-received TaC (Figure B.3) show that significant densification starts to occur only above 1950ºC, with density continuing to increase with increasing hot pressing temperature. The relative density increased from 75% at 1900ºC to 96% at 2400ºC.

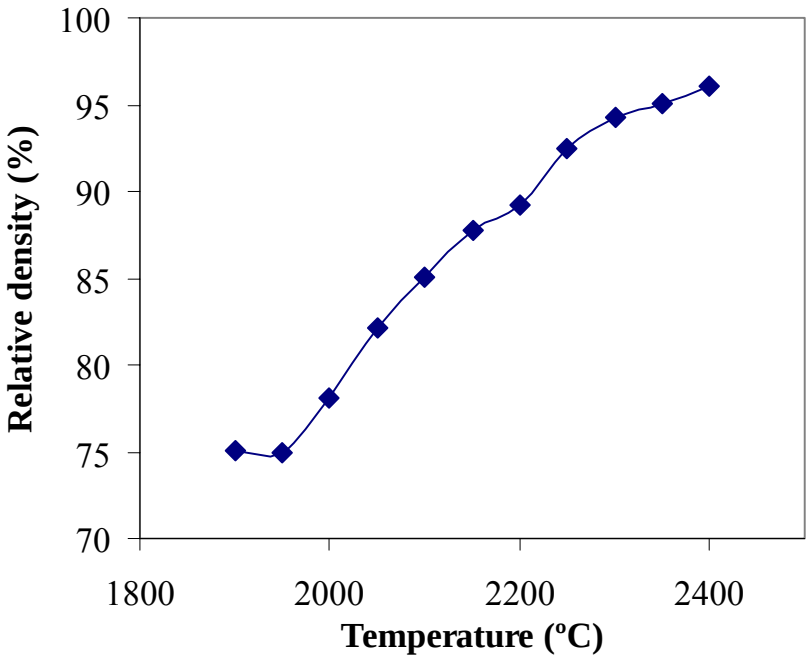

Figure B.3. Relative density as a function of hot pressing temperature for as-received TaC.

A SEM examination of the thermally etched cross-section of the TaC samples without additives (Figure B.4) revealed the development of the microstructures as a function of hot pressing temperature. The onset of neck growth between the particles started around 1900-1950ºC, which led to a highly porous structure with an intergranular network of interconnected pore channels. The amount of porosity decreased with increasing hot pressing temperature. In addition, the pores became rounded and isolated at multi-grain junctions at temperatures above 2100ºC. No measurable grain growth was observed for hot pressing temperatures up to 2300ºC, suggesting that transport mechanisms, such as grain boundary diffusion, that result in densification were dominant at these temperatures. Above 2300ºC grain growth had occurred. Grain growth appears to have been rapid at 2400ºC, since a significant fraction of the remaining porosity was entrapped within the grains, making it difficult to remove.

Densification of TaC with sintering additives

The addition of C and/or B_4C improved the densification of TaC significantly. The relative densities achieved with and without sintering additives were compiled in Figure B.5 for comparison. The relative density of pure TaC hot pressed at 2100ºC was 85%. The addition of 0.78 wt% C led to an increase in the relative density to 87% for the same hot pressing temperature. Additions of B_4C and B_4C-C were more effective than C alone in enhancing the densification of TaC. A relative density of 94% was achieved with 0.36 wt% B_4C additions and 96% with 0.43 wt% B_4C + 0.13 wt% C additions after hot pressing at 2100ºC. The highest density achieved with 0.78 wt% C addition was 97% at 2300ºC. A relative density of 98% was obtained with either 0.36 wt% B_4C or 0.43 wt% B_4C + 0.13 wt% C additions at 2200ºC.

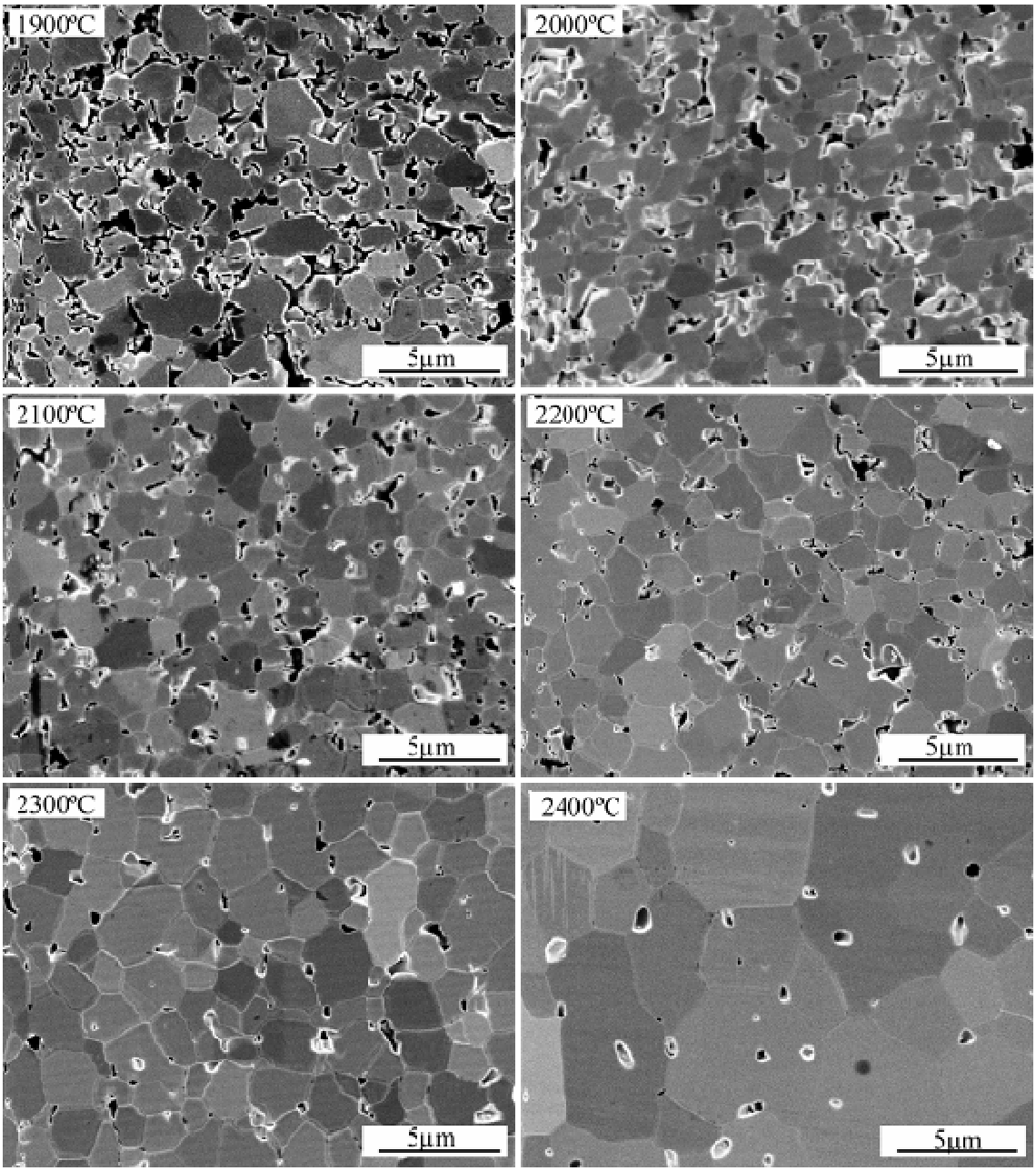

Figure B.4. SEM images of TaC without additives and hot pressed at 1900 to 2400ºC.

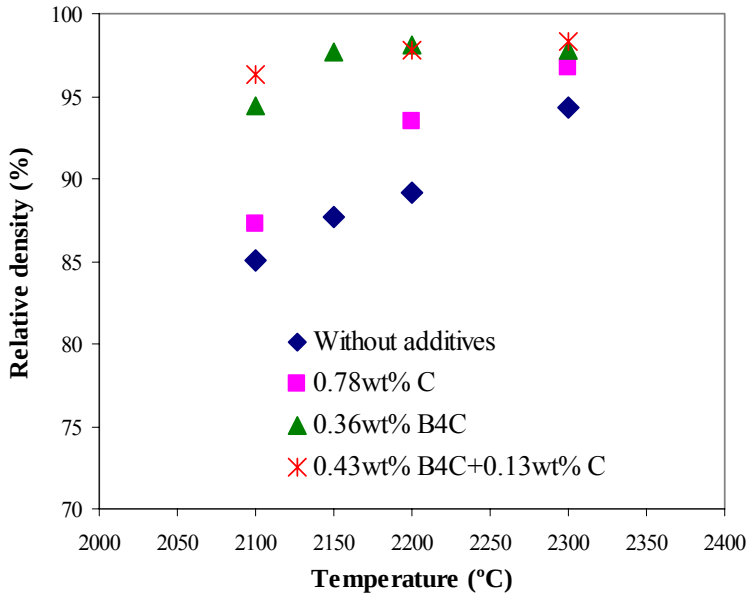

Figure B.5. Comparison of the relative densities of TaC vs. hot pressing temperature with and without B_4C and C additives.

The microstructures of the TaC samples with 0.78 wt% C additions (Figure B.6) were similar to the pure TaC, except for a visual reduction in the amount of porosity compared to samples fabricated at the same temperatures without additives. Hot pressing at 2000ºC produced a porous microstructure with intergranular porosity. While increasing temperature again reduced the level of porosity, grain growth was observed at 2300ºC, approximately 100ºC lower than the temperature for the onset of grain growth for TaC without C additions (2400ºC). However, most of the remaining porosity was still intergranular rather than intragranular. With 0.36 wt% B_4C additions, the microstructure changed significantly between 2100ºC and 2150ºC (Figure B.7). The porosity was intergranular, again with minimal or no grain growth up to 2100ºC. Rapid grain growth was observed at 2150ºC and higher temperatures, with the remaining porosity entrapped within the grains due to the considerable amount of grain growth. A similar SEM observation was made for TaC samples with 0.43 wt% B_4C + 0.13 wt% C additions processed at 2050-2300ºC (Figure B.8), except that rapid grain growth occurred at even lower temperatures (2100ºC) for this composition and resulted in entrapped porosity at 2100ºC and higher.

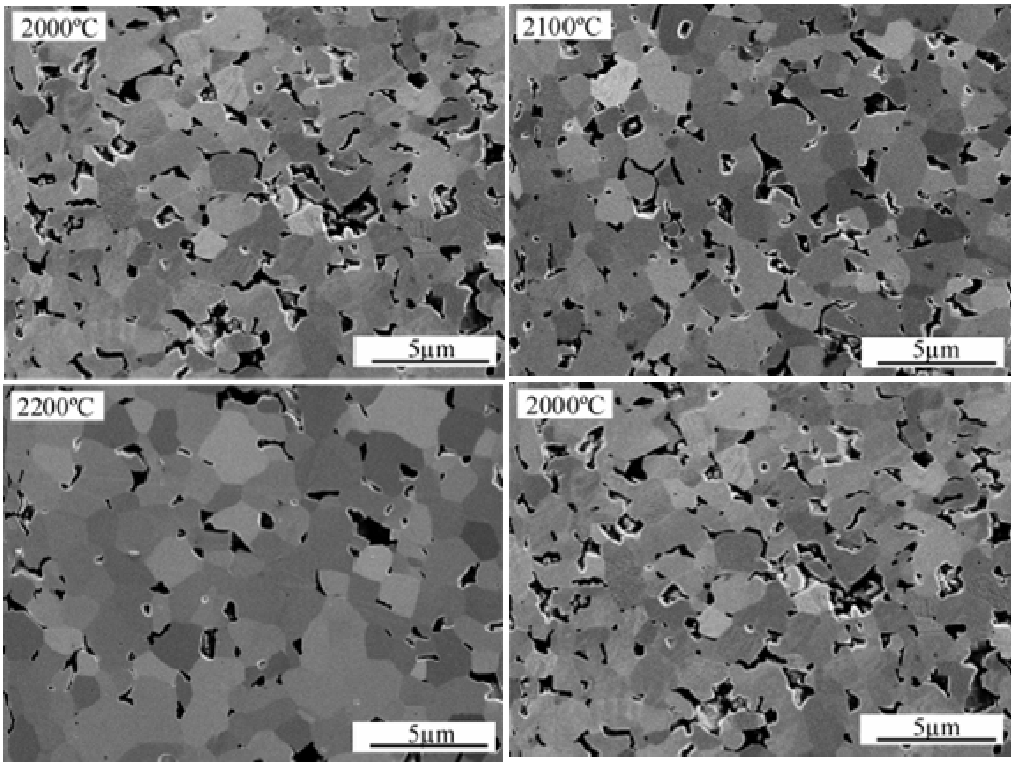

Figure B.6. SEM images of TaC with 0.78 wt% carbon additions hot pressed at 2000-2300ºC.

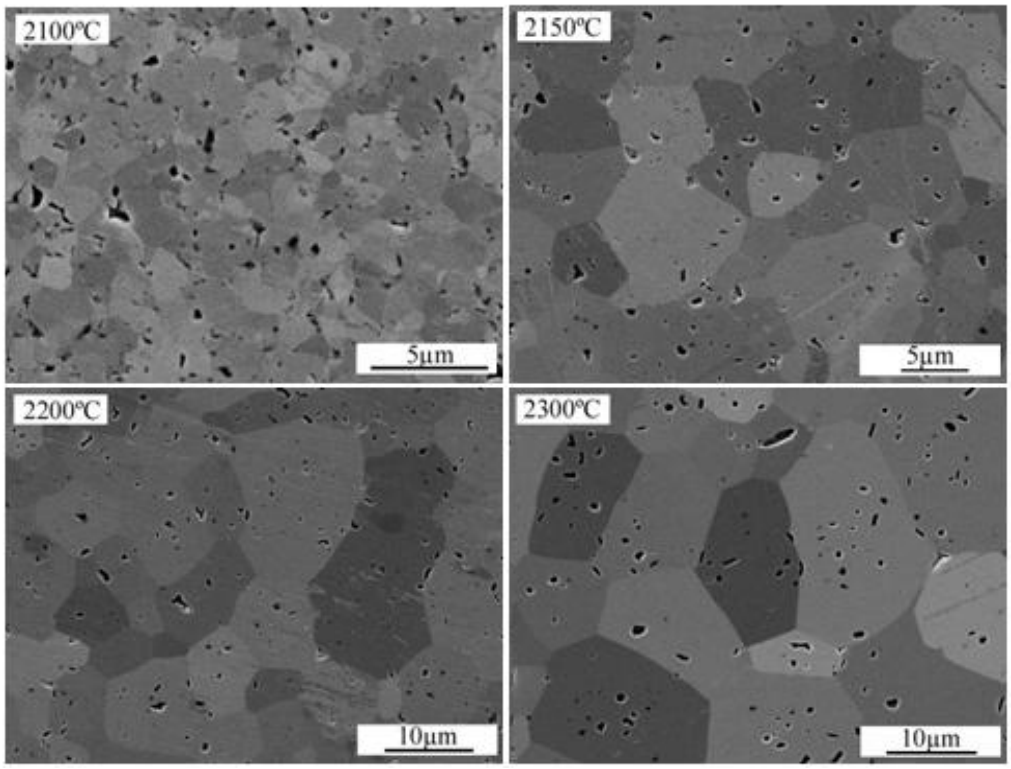

Figure B.7. SEM images of TaC with 0.36 wt% B_4C additions and hot pressed at 2100-2300ºC.

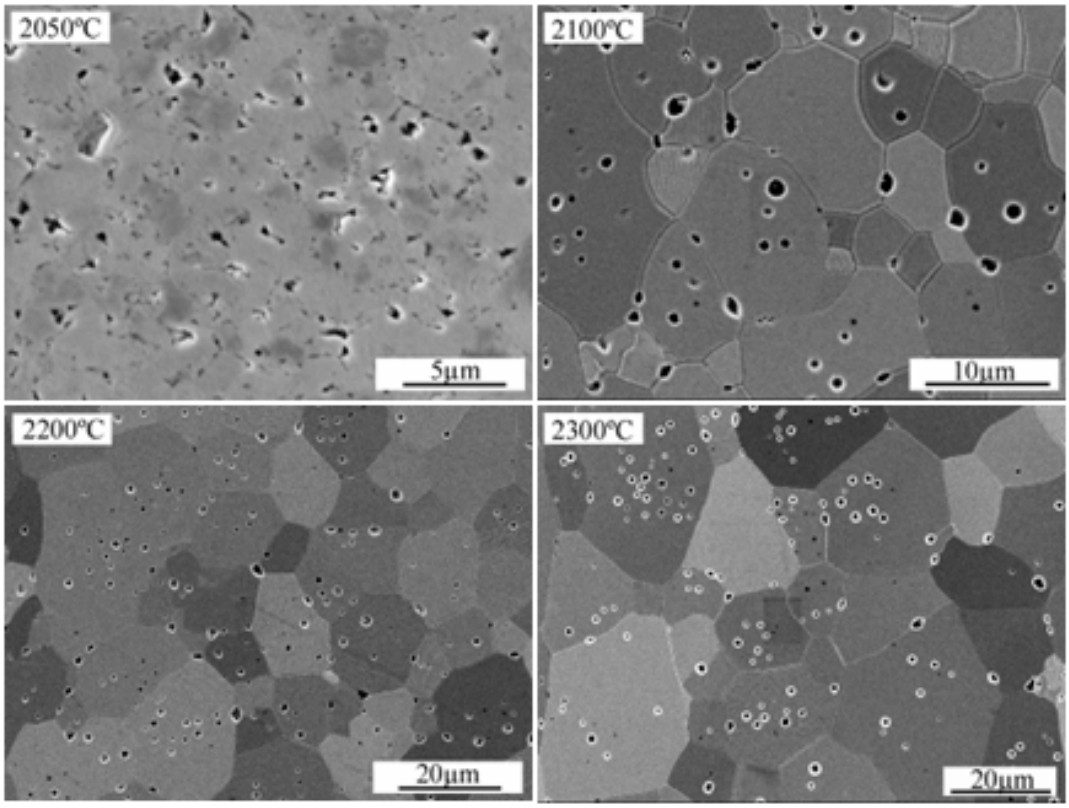

Figure B.8. SEM images of TaC with 0.43 wt% B_4C+0.13 wt% C additions hot pressed at 2050-2300ºC.

Discussion

The simultaneous occurrence of densification and grain growth in the hot pressed TaC ceramics produced in this study made it difficult to achieve ~100% density. Additions of C and/or B_4C reduced the onset temperature for both densification and grain growth of TaC. Grain growth did not initiate in the pure TaC until around 2300ºC. Alternatively, grain growth became significant at 2150ºC with 0.36 wt% B_4C additions and 2100ºC with 0.43 wt% B_4C + 0.13 wt% C additions. Additions of C and/or B_4C did not suppress the grain growth of TaC as had occurred in past studies for TiB_2[9], SiC[10], B_4C[11] ceramics. Rapid grain growth was found to reduce the driving force for densification and lead to entrapped porosity which was difficult to remove. No excess additives were observed in the microstructure of the compositions studied to date. Higher concentration of additives, or an additional high temperature additive, should be investigated to evaluate the effect of potentially pinning the growth of TaC grains at high temperature.

Characterization of TaC-based Monolithic and FM Samples with B_4C Additions

Monolithic samples with TaC + 2 wt% B_4C, hot pressed at UMR, were found to have a flexural strength of 590 MPa,[14] well above that reported for TaC hot pressed during the Phase I program, approximately 250 MPa. With such a significant improvement observed, the mechanical strength and microstructure of fibrous monolith samples with TaC containing this higher concentration of B_4C was evaluated. Also, monolithic samples of tertiary and quaternary blends fashioned around the TaC- HfC- VC systems studied in the Phase II were tested.

Binary Systems

Second pass FM samples with TaC-2 wt% B_4C as cell, and graphite as cell boundary, were prepared and hot pressed at 2100ºC, 4ksi at ACR. The FM sample configuration is as follows, with a final second pass filament extrusion diameter of 340μm.

17.5 vol% TaC + B_4C shell/ 82.5% core (17.5% graphite/ 82.5% TaC + B_4C)

The binary powder used in the FM sample preparation was prepared at UMR using attrition milling in hexane. The samples were machined to B-type bars for flexure strength tests. The first set of samples was mistakenly cut transversely, across the FM filaments. Flexure strength was measured in four-point bending in a mechanical load frame (Model 5881, Instron, Norwood, MA) at a crosshead speed of 0.5 mm/min. The strength was determined to be 64 ± 8 MPa (Table B.2) as an average of 8 bars. The microstructure of the fracture surfaces (Figure B.9) showed some porosity in the cells. The second set of samples, with the same compositions for the cells and cell boundaries, were cut longitudinally, with their long axis along the direction of the FM filaments. The flexure strength for these bars was determined to be 96 ± 25 MPa (Table B.2). No graceful failure was observed due to the fast crosshead speed. The microstructure (Figure B.10) revealed the cells and cell boundaries. Again, the cells were not fully dense.

Table B.2. Flexure strength of FM samples

Composition	Flexure strength (MPa)	
TaC + 2 wt% B_4C/ graphite	Longitudinal	Transverse
	96 ± 25	64 ± 8

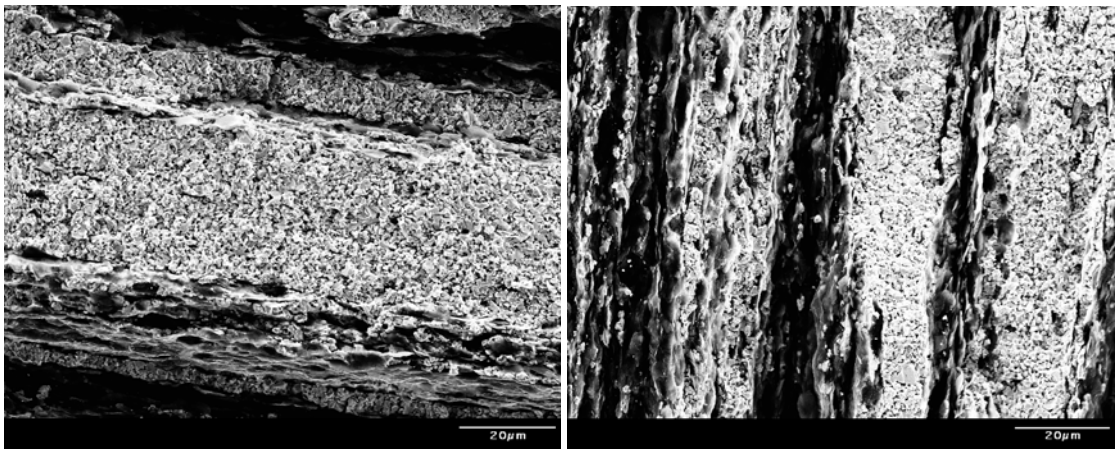

Figure B.9. Fracture surface of TaC + 2 wt% B_4C/ graphite FMs cut across filaments.

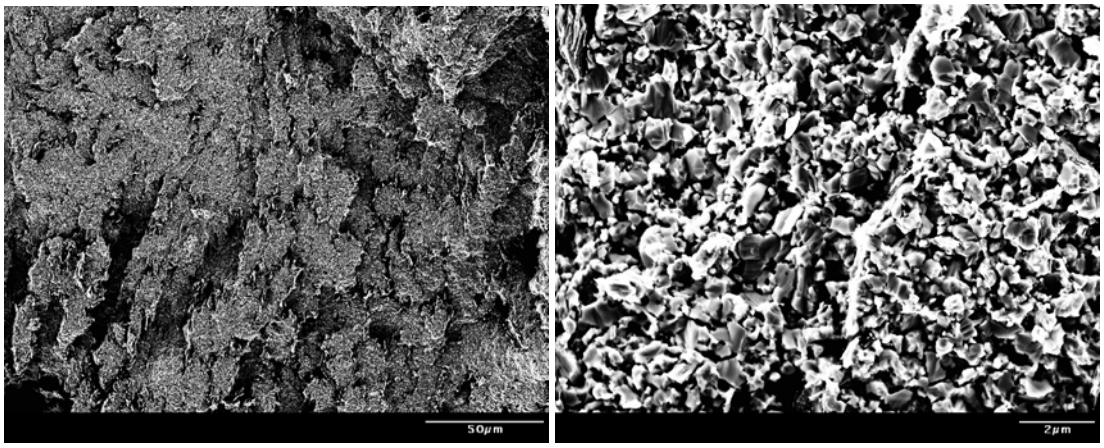

Figure B.10. Fracture surface of TaC + 2 wt% B_4C/ graphite FM cut along filaments.

Tertiary and Quaternary Systems

Tertiary and quaternary blends based on the TaC-rich material developed during the Phase II program were investigated. The addition of B_4C is intended to help control grain growth. This is the same motivation for using VC, which acts as a liquid sintering aid, reducing porosity. Because of this, blends with and without the VC component were evaluated. Powder blends were sent to UMR for milling according to the established procedure for the B_4C blends (SiC media, hexane) and returned to ACR for hot pressing.

Monolithic samples, described in Table B.3, were hot pressed at 2000 and 2100ºC at 6 ksi and returned to UMR for analysis. Small pieces (nominally 4 mm x 5 mm x 15 mm) were cut for analysis. Archimedes densities were measured. Samples from each hot pressing temperature were crushed and sieved for XRD analysis. The samples were polished for SEM microstructural observation and hardness measurements.

Table B.3. Compositions and hot pressing conditions.

Sample ID	TaC Blend Composition	Hot pressing temperature (ºC)
HP-1450	75.8 wt% TaC- 22.2% HfC- 2% B_4C	2000
HP-1451	75.8 wt% TaC- 22.2% HfC- 2% B_4C	2100
HP-1453	77.5 wt% TaC- 18.5%HfC- 2%VC- 2% B_4C	2000
HP-1452	77.5 wt% TaC- 18.5%HfC- 2%VC- 2% B_4C	2100

Results and discussion

Archimedes density

The bulk densities of the samples were measured using Archimedes' method with kerosene as the immersion medium. The true densities were calculated based on the rule of mixtures. The relative densities were then determined by the ratio of bulk density to true density. Table B.4 contains the results from the density measurements and calculations. The tertiary samples were 84.7% and 96.8% dense at 2000 and 2100ºC, respectively, while the quaternary samples were 89.3% and 100% dense at the same temperatures.

Table B.4. Bulk densities, true densities, and relative densities.

Sample ID	Bulk density (g/cm^3)	True density (g/cm^3)	Relative density (%)
HP-1450	10.5	12.4	84.7%
HP-1451	12.0	12.4	96.8%
HP-1453	10.8	12.1	89.3%
HP-1452	12.2	12.1	100%

Microstructural analysis of polished surfaces

The samples were polished to a 0.25 μm finish using successively finer diamond abrasives to reveal the porosity. The polished surface of the samples was observed by SEM (Hitachi S-570). Images of tertiary (Figure B.11) and quaternary (Figure B.12) samples hot pressed at 2000ºC showed some residual porosity, which is consistent with the trend in the Archimedes density measurements. Densification was not fully activated at this temperature. Samples hot pressed at 2100ºC were considerably more dense, with some dark grains distributed uniformly in a lighter matrix. The dark grains are most likely carbon based on our previous microstructural studies in the TaC + 2 wt% B_4C system. Thermodynamic calculations predict that reactions (see below) between TaC/ HfC/ VC and B_4C to form TaB_2/ HfB_2/ VB_2 and C are favorable over a wide range of temperatures (from 0-2500°C). However, due to the similar molecular weights between carbides and borides, it is difficult to differentiate the individual grains of the carbides versus borides, so we must also rely on XRD analysis.

$$2TaC + B_4C = 2TaB_2 + 3C$$
$$2HfC + B_4C = 2HfB_2 + 3C$$
$$2VC + B_4C = 2VB_2 + 3C$$

$\Delta G^0 < 0$ across the processing temperature range for all reactions

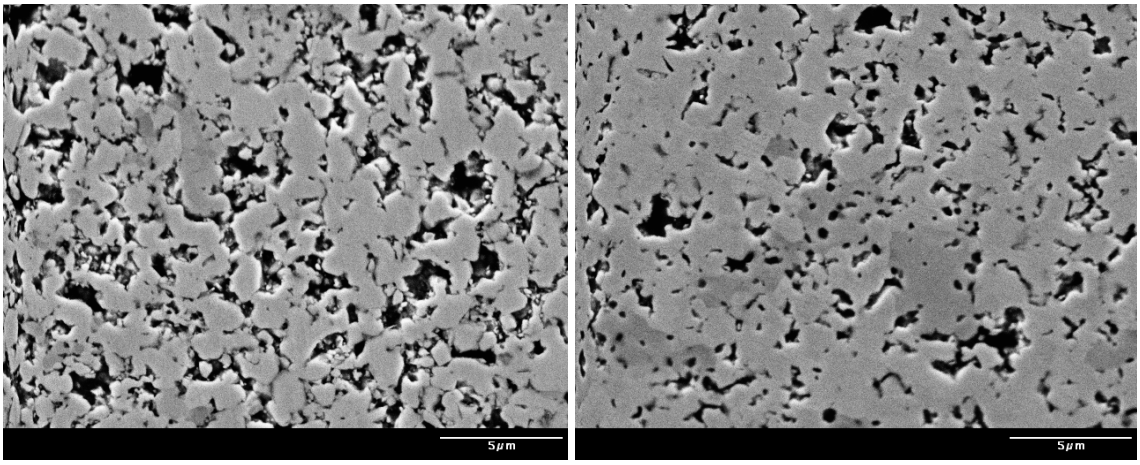

Figure B.11. SEM micrographs of polished surfaces of tertiary TaC-HfC-B_4C material hot pressed at 2000°C (left) and 2100°C (right).

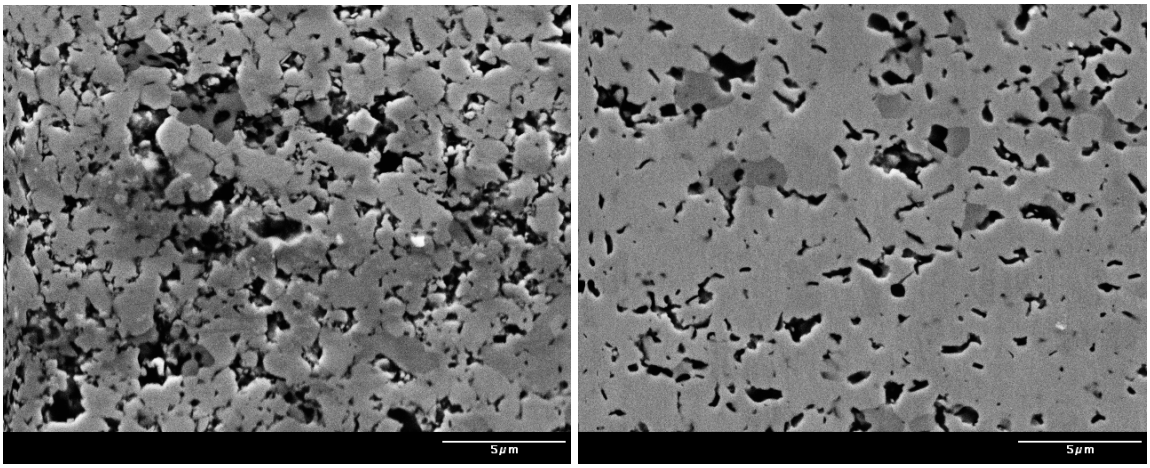

Figure B.12. SEM micrographs of polished surfaces of quaternary TaC-HfC-VC-B_4C material hot pressed at 2000°C (left) and 2100°C (right).

Microstructural analysis of thermal etched samples

The polished surfaces were then thermally etched at 1650ºC in argon for 1 hr and again examined by SEM to better reveal the grain boundaries of the materials. The microstructures (Figures B.13 and B.14) consisted of relatively large grains (~2 μm) surrounded by a higher percentage of submicron-sized grains which seemed to be recrystallized because the grain size was much smaller than the starting powders. There does not seem to be significant grain growth occurring between the two hot pressing

temperatures used. Carbides and borides could form their own solid solutions. Further, there might be some interaction between the carbides and the borides.

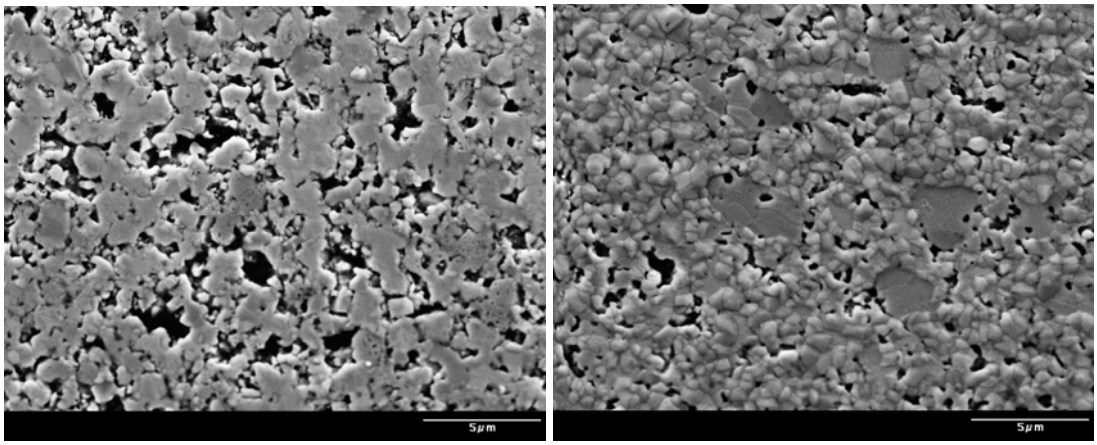

Figure B.13. SEM micrograph of thermally etched surface of tertiary TaC-HfC-B_4C material hot pressed at 2000°C (left) and 2100°C (right).

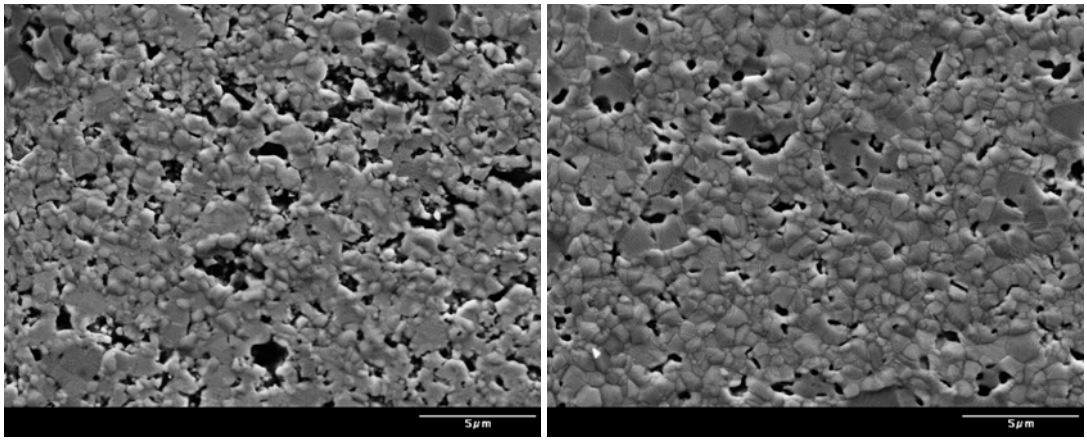

Figure B.14. SEM micrograph of thermally etched surface of quaternary TaC-HfC-VC-B_4C material hot pressed at 2000°C (left) and 2100°C (right)

XRD analysis

XRD analysis was performed to determine the phases present in the samples. The XRD patterns (Figure B.15) showed the presence of a trace phase, a boride, in addition to the major phase, TaC. The peaks for TaC are shifted slightly towards lower 2θ values, most likely due to the formation of a solid solution with both HfC and VC. The three carbides are all cubic in structure. The lattice parameter (Table B.5) for HfC (4.644Å) is slightly larger (~4%) than that of TaC (4.4555 Å), which is again larger than that of VC (4.160Å) by about 7%. The covalent radius (Table B.5) of Hf, Ta, and V decreases sequentially. Based on the similarity of the covalent radii and the lattice parameters, it appears that solid solutions should form readily among the three carbides, as expected. Since the TaC peaks are shifted to lower 2θ values, it would be expected that more HfC is in solid solution (larger radius) than VC, as expected based on the composition of the sample. The trace boride phase was different for each composition and hot pressing temperature.

Both the tertiary and quaternary blends formed HfB_2 at 2000ºC. TaB_2 was formed in the quaternary blend hot pressed at 2100ºC. For the tertiary blend hot pressed at 2100ºC, the peak cannot be attributed to a single boride. It is most likely a solid solution of HfB_2 and TaB_2. The three borides, like the carbides, have a similar structure (hexagonal). Their lattice parameters (Table B.6) are similar and will allow the formation of extensive solid solutions. Based on the XRD results, HfB_2 seems to form preferentially at lower temperatures while TaB_2 is formed at higher temperatures, which is likely related to the kinetics of the reactions.

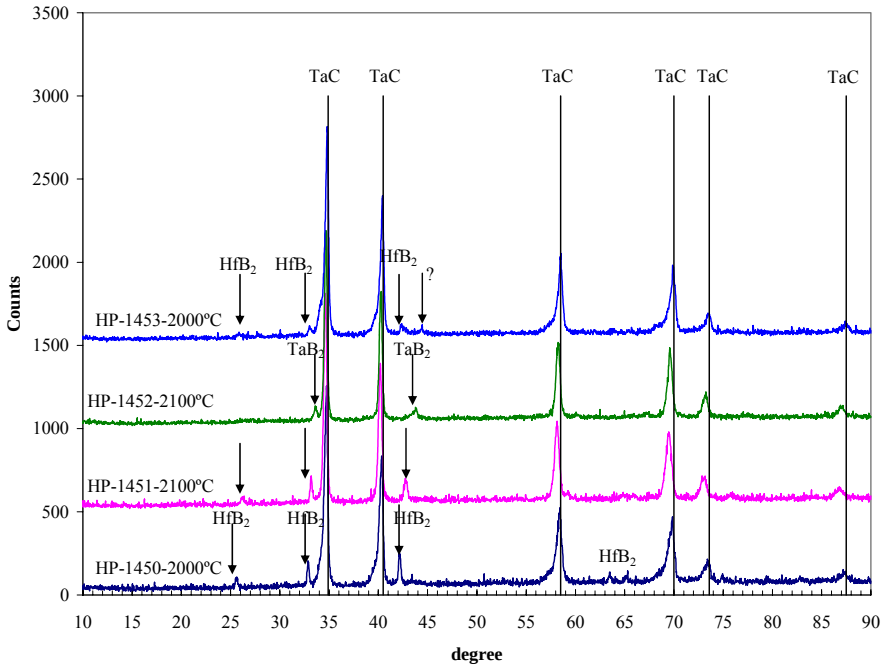

Figure B.15. XRD patterns of HP-1450, 1451, 1452, and 1453.

Table B.5. Lattice parameters of pure carbides (cubic) and covalent radii of metals.

Material	**HfC**	**TaC**	**VC**
Lattice parameter (Å)	4.644	4.4555	4.160
Covalent radius of metal element (Å)	1.50	1.38	1.25

Table B.6. Lattice parameters of borides (hexagonal)

Material	**HfB_2**	**TaB_2**	**VB_2**
Lattice parameter, a (Å)	3.14245	3.088	2.99761
Lattice parameter, c (Å)	3.47602	3.241	3.05620

Hardness and Flexural Strength Measurements

Hardness and flexural strength of the tertiary and quaternary samples were measured and are presented below in Table B.7. The hardness of the samples was measured using a

200g load on a microhardness tester (Struers, Duramin-5, Ballerup, Denmark) equipped with a Vickers' diamond indenter. The microhardness values are the average of ten valid indentations. The hardness of the tertiary samples prepared at 2000 and 2100ºC was 6.8 and 17.4 GPa, respectively. The hardness of the quaternary samples prepared at 2000 and 2100ºC was 8.2 and 22.6 GPa, respectively. Flexural strength was measured at ACR according to ASTM C1161, using a ramp speed of 0.50 mm/min. Strength values are the average for eight test specimens. The lower hardness and strength values of samples prepared at 2000ºC are attributed to the presence of porosity.

Table B.7. Hardness and flexural strength values.

Blend	Sample	Hot Press Temperature (°C)	Vicker's Hardness (GPa)	Flexural Strength (MPa)
TaC-HfC-B_4C	HP-1450	2000	6.8 ± 0.3	320 ± 38
	HP-1451	2100	17.4 ± 0.9	480 ± 69
TaC-HfC-VC-B_4C	HP-1453	2000	8.2 ± 0.4	354 ± 40
	HP-1452	2100	22.6 ± 0.7	373 ± 65

Discussion

For monolithic samples, the best consolidation was observed at the higher hot pressing temperature. Moderate improvements in density and corresponding improvements in hardness were observed for the quaternary system compared to the tertiary one. This result suggests that the liquid sintering component, VC, has a beneficial impact on mechanical strength.

Appendix C: Materials Used

Material	Supplier	Description	Part ID
Tantalum carbide, TaC	Atlantic Equipment Engineers (AEE)	99.8% pure, 1-5 μm	TA-301
Hafnium carbide, HfC	AEE	99.9% pure, -325 mesh	HF-301
Vanadium carbide, VC	AEE	99.8% pure, 1-5 μm	V-301
Boron carbide, B4C	H.C. Starck	0.8 μm	Grade HS
Graphite	Timcal	6.5 μm, irregular spheroid	TIMREX KS-6
Ethylene Ethyl Acrylate, EEA	DuPont	MFI 1.5 and 20	DPDA 9169 NT
Stearic Acid	Crompton		Hystrene 97 18 NF FG

References

1. J. B. Wachtman, *Mechanical Properties of Ceramics*, John Wiley & Sons, INC. 1996. p84.

2. G.V. Samsonov and R.Ya. Petrikina, "Sintering of Metals, Carbides, and Oxides by Hot Pressing," *Physics of Sintering*, 2[3], 1-20, 1979.

3. W.C. Yohe and A.L. Ruoff, "Ultrafine Grain Tantalum Carbide by High Pressure Hot Pressing," *Ceramic Bulletin*, 57[12], 1123-1130, 1978.

4. M.H. Leipold and P.F. Becher, "Pressure Densification in Tantalum Carbide," *Ceramic Bulletin*, 49[7], 647-651,1970.

5. J.J. Fischer, "Hot Pressing Mixed Carbides of Ta, Hf, and Zr," *Ceramic Bulletin*, 43[3] 183-185 (1964).

6. E. Roeder and M. Klerk, "Studies with the Electron Beam Microanalyzer on Hot Pressed Tantalum Carbide Having Small Additions of Manganese and Nickel," *Zeitschrift fuer Metallkunde*, 54, 462-70 (1963).

7. S. Scholz, "Some New Aspects of Hot Pressing of Refractories," *Special Ceramics*, p 293-305, ed. P.Popper, Academic Press, 1963.

8. L.E.Toth, Transition Metal Carbides and Nitrides, Academic Press, p148, 1971.

9. D.C. Halverson, A.J. Pyzik, I.A. Aksay, and W.E. Snowden, "Processing of Boron Carbide-Aluminum Composites," *J. Am. Ceram. Soc*., 72 [5] 775-80 (1989).

10. S. Baik and P.F. Becher, "Effect of Oxygen Contamination on Densification of TiB_2", *J. Am. Ceram. Soc.*, 70 [8] 527-530 (1987).

11. W.J. Clegg, "Role of Carbon in the Sintering of Boron-Doped Silicon Carbide", *J. Am. Ceram. Soc*., 83 [5] 1039-43 (2000).

12. H. Lee and R.F. Speyer, "Pressureless Sintering of Boron Carbide," *J. Am. Ceram. Soc*., 86 [9] 1468-73 (2003).

13. S.C. Zhang, G.E. Hilmas, and W.G. Fahrenholtz, "Pressureless Densification of Zirconium Diboride with Boron Carbide Additions," *J. Am. Ceram. Soc.*, 89 [5] 1544–1550 (2006).

14. Personal email correspondence, Xiaohong Zhang, May 6, 2007.